Acta Crystallographica Section A
Foundations of Crystallography
ISSN 0108-7673

Received 30 July 2004
Accepted 29 September 2004

Structures and phase transitions in perovskites – a group-theoretical approach[1]

Christopher J. Howard[a,b]* and Harold T. Stokes[c]

[a]Australian Nuclear Science and Technology Organisation, Private Mail Bag 1, Menai, NSW 2234, Australia, [b]School of Physics, The University of Sydney, Sydney, NSW 2006, Australia, and [c]Department of Physics and Astronomy, Brigham Young University, Provo, Utah 84602-4675, USA. Correspondence e-mail: cjh@ansto.gov.au

Applications of computer-based group-theoretical methods to perovskite crystallography are reviewed. Such methods furnish a systematic account of the effects on the high-symmetry parent structure of diverse distortions. New results are presented for elpasolites (ordered double perovskites) when both ferroelectric cation displacement and simple octahedral tilting are allowed. Group-theoretical results prove invaluable in assisting experimental studies of perovskites since, if the nature of the distortion is known, they limit the possible structures or, in relation to more extensive studies, constrain the sequences of structures that may occur. Spontaneous strains and the estimation of order parameters are briefly discussed. Group-theoretical methods are undoubtedly a powerful aid to the study of perovskite crystallography, and their computer implementation makes them more accessible than hitherto.

1. Introduction

Though the basic perovskite ABX_3 structure was established long ago (Kay & Bailey, 1957), the perovskite family (Mitchell, 2002) has held the interest of crystallographers to the present day (Glazer, 1972, 1975; Megaw, 1973; Thomas, 1989, 1996; Burns & Glazer, 1990; Woodward, 1997*a*,*b*). Structural variation in this family is often subtle, so the variants may differ only slightly from the cubic aristotype. This can make the determination of symmetry and structure a quite challenging task. Associated with the structural variation are structural phase transitions, occurring in response to changes in temperature, pressure or composition. The detailed study of such transitions, including a determination of the structures involved, represents another interesting if testing activity.

Interest in perovskites is by no means restricted to their crystallography. Perovskites exhibit a range of electrical and magnetic properties, giving rise to important actual and potential applications. For example, $BaTiO_3$ is ferroelectric at room temperature, with high dielectric constant, and is the major constituent of multilayer ceramic capacitors. These capacitors are delivering miniaturization to the electronics industry, being employed in lightweight notebook computers and mobile phones. $BaTiO_3$ is also used for thermistor devices, the electrical resistance increasing sharply at temperatures above the tetragonal to cubic phase transition. Lead zirconate titanate ($PbZrO_3$–$PbTiO_3$, abbreviated PZT), is another perovskite in widespread use. This is ferroelectric at room temperature, with good piezoelectric response, and has long found application both as sensor (*e.g.* sonar detector, piezoelectric gas igniter) and actuator (*e.g.* precision positioning devices, advanced fuel injectors, certain inkjet printers). The piezoelectric response of PZT is intimately linked to its crystal structure, and best performance is achieved in compositions close to a phase boundary (Newnham, 1998). Tungsten trioxide, WO_3, a semiconductor, and structurally a close relative of perovskite, is the active material in electrochromic windows. Certain more complex perovskites find application as microwave resonators, on account of their high relative permittivity, low dielectric loss, and near-zero temperature coefficient of resonant frequency (Kawashima *et al.*, 1983). Future applications of perovskites are indicated by current research. Thin films of Cr-doped $SrTiO_3$ and $SrZrO_3$, for example, are being studied (Beck *et al.*, 2000) for their potential in non-volatile computer memories. The majority of materials exhibiting a giant magnetoresistive response (Gong *et al.*, 1995) are perovskites, and the now famous high-temperature oxide superconductors (Cava *et al.*, 1987; Capponi *et al.*, 1987) still under intensive investigation are also generally considered as members of the extended perovskite family (Mitchell, 2002). Finally, we remark on the importance of perovskites in the earth sciences. Magnesium silicate in particular, $MgSiO_3$, is considered to adopt the perovskite structure in the earth's lower mantle, making silicate perovskites the most abundant minerals on earth (Ringwood, 1962; Mitchell, 2002). The influence of phase transitions on the elastic constants of lower mantle perovskites may be of

[1] This article is dedicated to Helen D. Megaw (1907–2002), in appreciation of her many contributions to the crystallography of inorganic and mineral compounds, including her seminal studies of perovskites. Some of the material was presented by CJH in the Megaw memorial session at the 21st European Crystallography Meeting, Durban, South Africa, August 2003.

particular significance in seismology (Carpenter & Salje, 1998). There are reasons aplenty for investigations of perovskites to be continued.

The structure of the ideal perovskite is cubic, with space-group symmetry $Pm\bar{3}m$, and has been described (Megaw, 1973) as 'probably the simplest example of a structure containing two different cations'. The only variable parameter in this ideal cubic structure is the lattice parameter, and for only rather few combinations ABX_3 (*e.g.* $SrTiO_3$ at room temperature) is the ideal structure formed. The structure can however be distorted to accommodate a much wider range of ions, and indeed most perovskites have lower symmetry than the aristotype. Three different distortions have been identified (Megaw, 1973): distortions of the BX_6 octahedral units, *B*-cation displacements within these octahedra, and the tilting of the BX_6 octahedra relative to one another as practically rigid corner-linked units. These different kinds of distortion can occur separately or in combination. If we add the possibilities of more than one cation on the *A* or *B* sites, and more than one anion on the *X* site, and of the ordering of these different cations/anions in the pertinent sites, then many different structures are produced. It is said (Mitchell, 2002) that every element of the Periodic Table, with the exception of the noble gases, can be found in some perovskite or perovskite variant.

The investigation of perovskite structures can be greatly assisted by prior analysis of the distortions involved and the structures that might result. The idea is to simplify the crystallographic problem by limiting the number of solutions. The analysis can also lead to an understanding of the inter-relationship between the different structures, and the nature, continuous or otherwise, of any transitions that occur between them. This provides a valuable reference when phase transitions are under study. In our own studies of perovskites (Howard & Stokes, 1998; Howard *et al.*, 2002; Stokes *et al.*, 2002; Howard *et al.*, 2003; Howard & Zhang, 2004*a*,*b*), we used group-theoretical methods to enumerate the possible structures, and to examine the relationships between them. The methods used for finding *isotropy subgroups* were those developed by Hatch and Stokes (Hatch, 1984; Stokes & Hatch, 1984, 1985; Hatch & Stokes, 1985, 1986, 1987*a*,*b*; Hatch *et al.*, 1987) and implemented in the computer program *ISOTROPY* (http://stokes.byu.edu/isotropy.html). This group-theoretical approach might be considered as a formal development from the ideas advanced by Megaw (1973) some 30 years ago.

Guided by results from group-theoretical analyses, we have carried out a number of experimental studies on structures and structural phase transitions in perovskites (see for example Kennedy, Prodjosantoso & Howard, 1999; Howard, Kennedy & Chakoumakos, 2000; Howard, Knight *et al.*, 2000; Moussa *et al.*, 2001; Howard *et al.*, 2001, 2002; Howard & Zhang, 2003; Carpenter *et al.*, 2005). For the most part, we have used high-resolution X-ray and neutron powder diffraction techniques. Diffraction patterns from distorted perovskites will show splitting of the main perovskite peaks and/or additional superlattice peaks, but since the distortions are often subtle the splitting may be slight and the superlattice peaks weak. Thus, high resolution may be required to resolve the peak splitting, while neutron diffraction can be advantageous when only the lighter elements contribute to the superlattice peaks. Order parameters for phase transitions can be derived from either atomic coordinates or spontaneous strains. In the case of temperature-induced phase transitions, the use of fine temperature steps has enabled us to better judge the nature (*e.g.* continuous or discontinuous) of the phase transition. The use of powder diffraction techniques relates to the difficulty of obtaining good monodomain single crystals – even if the cubic phase can be obtained in single-crystal form, it is likely that the crystal will comprise multiple domains below any phase transition that occurs. In certain cases (see for example Howard *et al.*, 2001), a single domain can be examined using electron diffraction with small probe size and, since the superlattice peaks are readily seen in electron diffraction, this method becomes a powerful aid to the determination of space-group symmetry.

In this paper, we shall endeavour to explain how to enumerate the structures of distorted perovskites using the group-theoretical methods implemented in computer program *ISOTROPY*. We suggest that this program makes these methods more accessible than hitherto. The analysis involves first the association with each distortion of an irreducible representation (irrep) of the parent space group $Pm\bar{3}m$, then the listing of all the isotropy subgroups corresponding to the irrep or irreps involved, an inspection of these results for group–subgroup relationships, and finally for each group–subgroup pair a determination as to whether the corresponding phase transition is allowed to be continuous. Program *ISOTROPY* is used at every step. A number of experimental investigations will be reviewed, with particular emphasis on cases in which the group-theoretical analysis contributed significantly to structure solution.

2. Group-theoretical analysis

In this section, we shall describe the various steps in the group-theoretical analysis, and indicate how they are implemented using *ISOTROPY*. It is first necessary to clarify the description of the structure of the perovskite aristotype.

2.1. The ideal perovskite

The ideal perovskite ABX_3 is cubic, in space group $Pm\bar{3}m$ (Fig. 1). The structure is commonly visualized as a three-dimensional network of regular corner-linked BX_6 octahedra, the *B* cations being at the centre of these octahedra and the *A* cations being centrally located in the spaces between them. There is more than one way of setting the perovskite in its space group. We set the octahedrally coordinated *B* cation at Wyckoff 1*a*, 0, 0, 0, the *A* cation at 1*b*, 1/2, 1/2, 1/2, and the anion *X* at 3*d*, 1/2, 0, 0. Strontium titanate, $SrTiO_3$, cubic with lattice parameter $a = 3.905$ Å at room temperature, represents an example of the ideal perovskite.

2.2. *B*-cation displacement (ferroelectric)

As recognized by Megaw (1973), *B* cations can be displaced from the centres of the BX_6 octahedra. If all *B* cations are equally displaced, we have the technically important case of ferroelectricity, such as manifested in $BaTiO_3$. This also provides a simple yet non-trivial illustration of the application of group theory to distorted perovskites.

The *B* cation, originally at 0, 0, 0, can be displaced in some arbitrary direction from the centre of the BX_6 octahedron. We use symbols φ_1, φ_2, φ_3 to denote unit displacements in the [100], [010], [001] directions, respectively. There is no imperative that the magnitudes of the displacements in these different directions should be equal. The operation on φ_1, φ_2, φ_3 of any element g of the parent space group $G_0 = Pm\bar{3}m$ produces linear combinations of these basic displacements, according to

$$g(\varphi_1, \varphi_2, \varphi_3) = (\varphi_1, \varphi_2, \varphi_3)D(g), \tag{1}$$

where $D(g)$ is a 3×3 matrix. For any $g_1, g_2 \in G_0$, we find $D(g_1g_2) = D(g_1)D(g_2)$, which implies the set of matrices $D(g)$ carried by the basis functions φ_1, φ_2, φ_3 form a *representation* of the group G_0. Of course, the identity operation ($g = E$) must leave everything unchanged and, since all *B* cations are equally displaced, so too must every lattice translation. Clearly, the inversion operation ($g = I$) will take each of the unit displacements into its negative. Rotation by $\pi/2$ around the z axis ($g = C_{4z}^{+}$) carries the unit displacement in the x direction to the y direction, and the unit displacement in the y direction to the unit negative displacement along the x direction, leaving the displacement along the z direction unchanged. A positive rotation around the threefold axis, [111], ($g = C_{31}^{+}$) will carry unit displacement along the x direction to the y direction, unit displacement along the y direction to the z direction, and unit displacement along the z direction to the x direction. Based on these arguments, we find

$$D(E) = \begin{pmatrix} 1 & 0 & 0 \\ 0 & 1 & 0 \\ 0 & 0 & 1 \end{pmatrix}, \quad D(I) = \begin{pmatrix} -1 & 0 & 0 \\ 0 & -1 & 0 \\ 0 & 0 & -1 \end{pmatrix},$$

$$D(C_{4z}^{+}) = \begin{pmatrix} 0 & -1 & 0 \\ 1 & 0 & 0 \\ 0 & 0 & 1 \end{pmatrix}, \quad D(C_{31}^{+}) = \begin{pmatrix} 0 & 0 & 1 \\ 1 & 0 & 0 \\ 0 & 1 & 0 \end{pmatrix}. \tag{2}$$

Proceeding with similar arguments, or simply by multiplying the matrices corresponding to the generators (C_{4z}^{+}, C_{31}^{+}, I) of G_0, we obtain a mapping of all elements $g \in G_0$ onto a set of 3×3 matrices forming a representation of G_0. This can be identified by reference to tables (Miller & Love, 1967) as the three-dimensional *irreducible representation* (irrep) Γ_4^-. This is the required association of an irrep of $Pm\bar{3}m$ with the distortion under consideration.

Next we define an 'order parameter' $\boldsymbol{\eta} = (\eta_1, \eta_2, \eta_3)$[2] where η_i represents the magnitude (and sign) of the displacement in the direction of the basis function φ_i. A general displacement φ can be written in terms of the basic displacements and the order parameter

$$\varphi = \sum_i \varphi_i \eta_i. \tag{3}$$

An operation on φ by an element $g \in G_0$ results in

$$g\varphi = g(\varphi_1, \varphi_2, \varphi_3)\begin{pmatrix} \eta_1 \\ \eta_2 \\ \eta_3 \end{pmatrix} = (\varphi_1, \varphi_2, \varphi_3)D(g)\begin{pmatrix} \eta_1 \\ \eta_2 \\ \eta_3 \end{pmatrix}. \tag{4}$$

From the form of this equation, it is apparent that we can take the basis functions as fixed, and consider $g \in G_0$ as acting on the order parameter rather than on the basis functions themselves, so that

$$g\begin{pmatrix} \eta_1 \\ \eta_2 \\ \eta_3 \end{pmatrix} = D(g)\begin{pmatrix} \eta_1 \\ \eta_2 \\ \eta_3 \end{pmatrix} \tag{5}$$

and the order parameter space carries the representation Γ_4^-.

A particular displacement of the *B* cation is described by a particular value of the order parameter $\boldsymbol{\eta}$, and the operation g carries this to another possibly different displacement $g\boldsymbol{\eta}$. The symmetry of the structure is determined by those $g \in G_0$ that leave the displacement (and hence the structure as a whole) invariant, that is for which

$$g\boldsymbol{\eta} = \boldsymbol{\eta}. \tag{6}$$

These operations form a space group G termed an *isotropy subgroup* of G_0. We consider the specific case in which the displacement is along the z axis, so $\boldsymbol{\eta} = (0, 0, \eta_3)$. Referring to the example matrices in equation (2), we find $g = E$ and $g = C_{4z}^{+}$ leave $\boldsymbol{\eta}$ unchanged, whereas $g = I$ and $g = C_{31}^{+}$ do not. Every element of $g \in G_0$ is examined in this way, and it is found that the space group comprising the elements that leave the displacement invariant is the space group $G = P4mm$. As will be explained below, this result can be obtained quickly using

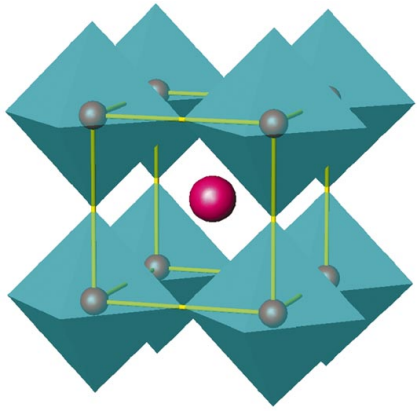

Figure 1
Schematic of the $Pm\bar{3}m$ perovskite, for example $SrTiO_3$, including an outline of the cubic unit cell. The BX_6 units are represented as octahedra, the *B* atoms being visible within them, and the *X* atoms considered to lie at the vertices. The *A* ion is centrally located in the cubo-octahedral cavity between the octahedra.

[2] The order parameter is a column vector, but for compactness when it is in the text we write it as a row.

Table 1
Structures derived from the ideal perovskite in $Pm\bar{3}m$ by displacement of the B cation.

The active irrep is Γ_4^- ($\boldsymbol{k}$ = 0,0,0). Different values for the order parameter correspond to different directions of cation displacement. We show, for each structural derivative, the space-group symmetry (and space-group number) along with the lattice vectors and origin referred to the lattice vectors and origin of the $Pm\bar{3}m$ parent structure.

Order parameter	Space group	Basis vectors	Origin
(0,0,0)	$Pm\bar{3}m$ (No. 221)	(1,0,0), (0,1,0), (0,0,1)	(0,0,0)
(0,0,a)	$P4mm$ (No. 99)	(1,0,0), (0,1,0), (0,0,1)	(0,0,0)
(a,a,0)	$Amm2$ (No. 38)	(0,0,1), (1,$\bar{1}$,0), (1,1,0)	(0,0,0)
(a,a,a)	$R3m$ (No. 160)	(1,$\bar{1}$,0), (0,1,$\bar{1}$), (1,1,1)	(0,0,0)
(a,b,0)	Pm (No. 6)	(0,1,0), ($\bar{1}$,0,1), (1,0,0)	(0,0,0)
(a,a,b)	Cm (No. 8)	(1,1,0), ($\bar{1}$,1,0), (0,0,1)	(0,0,0)
(a,b,c)	$P1$ (No. 1)	(1,0,0), (0,1,0), (0,0,1)	(0,0,0)

program *ISOTROPY*. We shall also use the program to find other isotropy subgroups corresponding to different choices for the order parameter, and the results are summarized in Table 1.

Barium titanate is known to adopt the structures in $R3m$, $Amm2$, $P4mm$ and $Pm\bar{3}m$, depending on temperature (Kay & Vousden, 1949; Darlington *et al.*, 1994).

A list of isotropy subgroups, such as appears in Table 1, can be examined for group–subgroup relationships. These relationships can be established on the basis of the order parameters. For example, if we consider (a,a,0) and (a,a,b), these span respectively one- and two-dimensional subspaces of order parameter space, and the two-dimensional space includes the one-dimensional space. Clearly, all those elements $g \in G_0$ satisfying $g\boldsymbol{\eta} = \boldsymbol{\eta}$ when $\boldsymbol{\eta} = (a, a, b)$ will also satisfy this condition when $\boldsymbol{\eta} = (a, a, 0)$, so the isotropy subgroup Cm corresponding to (a, a, b) must be a subgroup of $Amm2$ corresponding to $(a, a, 0)$. The argument can be written more generally as follows. If the subspace spanned by a particular order parameter is of a higher dimension than that spanned by another order parameter, but *includes* the subspace spanned by the second order parameter, then the isotropy subgroup associated with the second order parameter is a subgroup of that associated with the first order parameter. We have applied this argument in all our previous work (Howard & Stokes, 1998; Howard *et al.*, 2002; Stokes *et al.*, 2002; Howard *et al.*, 2003; Howard & Zhang, 2004*a*,*b*; Howard & Stokes, 2004). The group–subgroup relationships from Table 1 can be illustrated in a tree, shown here as Fig. 2.

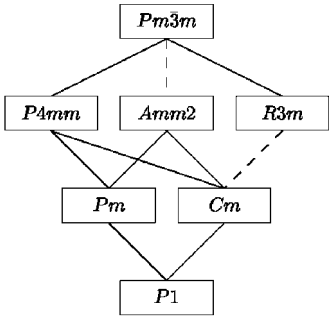

Figure 2
A schematic diagram showing the group-subgroup relationships among the seven space groups listed in Table 1. The lines indicate group–subgroup relationships – a dashed line indicates that, according to Landau theory, the corresponding phase transition cannot be continuous.

A final point of interest, of particular relevance to the study of phase transitions, is whether the phase transition corresponding to a particular group–subgroup pair is allowed to be continuous. (A transition that does not correspond to a group–subgroup pair cannot be continuous.) This assessment depends for example on Landau theory (Landau & Lifshitz, 1980). Considering a temperature-induced transition, we can expand the excess free energy for transitions from $Pm\bar{3}m$ associated with B-cation displacement as

$$G = \tfrac{1}{2}A(T - T_c)(\eta_1^2 + \eta_2^2 + \eta_3^2) + \tfrac{1}{4}B(\eta_1^2 + \eta_2^2 + \eta_3^2)^2 + \tfrac{1}{4}B'(\eta_1^4 + \eta_2^4 + \eta_3^4) + \tfrac{1}{6}C(\eta_1^2 + \eta_2^2 + \eta_3^2)^3 + \ldots, \quad (7)$$

where A, B, B', C are presumed constant. The expansion should be valid for small values of the order parameter. The excess free energy is determined largely by long-range elastic interactions, except for the term containing T, which is an entropy term. It must be invariant under all the operations $g \in G_0$, and to achieve this each term in the expansion has been constructed from an invariant. The expansion is in effect a 2–4–6 potential and, for $A > 0$ and $B > 0$, continuous phase transitions would be expected (Salje, 1990). Indeed, if we were to take only the first two terms and write them in terms of the squared magnitude of the order parameter, $\eta^2 = \eta_1^2 + \eta_2^2 + \eta_3^2$, we would find from the condition for a minimum $\partial G/\partial\eta = 0$, for temperatures below the phase transition,

$$\eta^2 = A(T_c - T)/B, \quad (8)$$

as would be the classic form for a second-order phase transition. The effect of the term $\eta_1^4 + \eta_2^4 + \eta_3^4$ is to distinguish the different directions in order-parameter space since, for a given small value of η, it achieves maximum values for directions such as (η,0,0) and minimum values for directions like $(\eta,\eta,\eta)/\sqrt{3}$. It follows that the true minimum of G for small η will occur at (0,0,η) or $(\eta,\eta,\eta)/\sqrt{3}$ according as $B' < 0$ or $B' > 0$. There is no way that the true minimum can occur at $(\eta,\eta,0)/\sqrt{2}$. Comparing with the entries in Table 1, we see that we can have continuous transitions from $Pm\bar{3}m$ to either $P4mm$ (0,0,a) or $R3m$ (a,a,a), but that our free-energy expansion cannot account for a transition to $Amm2$ (a,a,0). Evidently, such a transition, if it occurs, cannot be described using the free-energy expansion for small values of the order parameter, so the transition could not be continuous. As to the other group–subgroup relationships indicated in Fig. 2, the expansion in the order parameter for the transition from $R3m$ to Cm is of the 2–3–4 type, leading to a first-order transition (Salje, 1990), whereas expansions for all the other transitions are of the 2–4–6 type without the subtleties encountered above, so all the other transitions are allowed to be continuous. We will refer again to the expansion (7) in §5.

We have identified the irrep, found one isotropy subgroup (listed others), identified group–subgroup relationships, and examined using Landau theory which transitions are allowed

to be continuous. We will now show how these various steps are completed with the aid of computer program *ISOTROPY*.[3]

The association of an irrep with the *B*-cation displacement is made quite readily using *ISOTROPY*. An approach closely resembling the one we have described above is reflected in the program run recorded (in its entirety) here (Fig. 3). We first set the parent space group as #221 ($Pm\bar{3}m$). Next we note that *B*-cation displacements identical at all *B* sites will not lead to any multiplication of the unit cell, so the distortion will be associated with the Γ point ($\boldsymbol{k} = 0,0,0$) of reciprocal space. The entry 'value kpoint gm' restricts the search to irreps associated with the Γ point. We then use 'show microscopic vector' to look for displacements at the Wyckoff *a* position – this is where the *B* cation is located – and find only irrep Γ_4^- produces displacements at this point. This is the required result.

The program can be run again, if desired, to examine the effect of irrep Γ_4^- at Wyckoff positions *b* and *d*, and it is found that the irrep can produce displacements at both positions. Note also that the program can accept abbreviated instructions (*e.g.* v par 221, d dis), provided only that these abbreviations do not result in ambiguity.

The next step is to list the isotropy subgroups of $Pm\bar{3}m$ for the irrep Γ_4^-. The dialogue is now almost self-explanatory. The instruction 'show direction vector' shows the order parameter for each of the isotropy subgroups. These include *P*4*mm* as we obtained above, although *ISOTROPY* has by default listed that domain with cation displacement in the *x* direction and fourfold axis [100]. We have used instructions 'show basis' and 'show origin' to obtain the origin and lattice vectors of each isotropy subgroup referred to the origin and lattice vectors of the $Pm\bar{3}m$ parent. It may be seen that we completed our Table 1 using the output (Fig. 4) from this run. The Wyckoff positions in each isotropy subgroup, given the Wyckoff position in the parent, can be printed if desired.

The recognition of group–subgroup relationships is based on the order parameters, and the process was fully explained above. The order parameters are listed by *ISOTROPY*, but the identification of group–subgroup relationships from these order parameters remains in most cases a manual process.

ISOTROPY can be used to examine the transition corresponding to any group–subgroup pair to determine whether the corresponding phase transition is allowed to be continuous. The pair is checked in Landau theory, and also against the more demanding requirement of renormalization group theory (Hatch *et al.*, 1986, and references therein). The instruction 'show continuous' can be used prior to 'display isotropy' to give the information required. The results for the transitions from $Pm\bar{3}m$ to *P*4*mm*, *Amm*2, *R*3*m* are immediately listed. For the other group–subgroup pairs, we might set 'value size 1' on the basis that the displacements under consideration do not multiply the size of the primitive unit cell, and examine each pair in turn. The program listing (Fig. 5) is in this case incomplete, and illustrates only the analysis of the *P*4*mm* to *Pm* and *R*3*m* to *Cm* group–subgroup pairs.

In our account of the use of program *ISOTROPY*, we have followed as closely as possible the same procedures as we did in our earlier more formal treatment. *ISOTROPY* does however offer a variety of other approaches to the problem. For example, if we started from the knowledge that the

```
Isotropy, Version 6.4.2, August 2000
Harold T. Stokes and Dorian M. Hatch
Brigham Young University
*DISPLAY SETTING
Current setting is International (new ed.) with conventional basis vectors.
*value parent 221
*value kpoint gm
*value wyckoff a
*show irrep
*show microscopic vector
*display distortion
Irrep (ML) Point   Mode Projected Vectors
GM4-       (0,0,0) 1    (1,0,0), (0,1,0), (0,0,1)
*quit
```

Figure 3
ISOTROPY dialogue. Finding the irrep that gives ferroelectric *B*-cation displacements.

```
Isotropy, Version 6.4.2, August 2000
Harold T. Stokes and Dorian M. Hatch
Brigham Young University
*DISPLAY SETTING
Current setting is International (new ed.) with conventional basis vectors.
*value parent 221
*value irrep gm4-
*show subgroup
*show direction vector
*show basis
*show origin
*display isotropy
Subgroup Dir         Basis Vectors              Origin
99 P4mm  P1  (a,0,0) (0,1,0), (0,0,1), (1,0,0)  (0,0,0)
38 Amm2  P2  (a,a,0) (0,0,1), (1,-1,0),(1,1,0)  (0,0,0)
160 R3m  P3  (a,a,a) (1,-1,0),(0,1,-1),(1,1,1)  (0,0,0)
6 Pm     C1  (a,b,0) (0,1,0), (0,0,1), (1,0,0)  (0,0,0)
8 Cm     C2  (a,a,b) (1,1,0), (-1,1,0),(0,0,1)  (0,0,0)
1 P1     S1  (a,b,c) (1,0,0), (0,1,0), (0,0,1)  (0,0,0)
*quit
```

Figure 4
Enumeration of the isotropy subgroups. Combining the elementary vector displacements from Fig. 3 as indicated by the order parameter listed here gives the cation displacement in each case.

```
.................
*value parent pm-3m
*value irrep gm4-
*show parent
*show subgroup
*show maximal
*show continuous
*display isotropy
Parent    Subgroup Max Cont
221 Pm-3m 99 P4mm  yes RG
221 Pm-3m 38 Amm2  yes no
221 Pm-3m 160 R3m  yes RG
221 Pm-3m 6 Pm     no  no
221 Pm-3m 8 Cm     no  no
221 Pm-3m 1 P1     no  no
.................
*cancel value irrep
*value size 1
*value parent p4mm
*value subgroup pm
*display isotropy
Parent  Subgroup Max Cont
99 P4mm 6 Pm     yes RG
.................
*value parent r3m
*value subgroup cm
*display isotropy
Parent  Subgroup Max Cont
160 R3m 8 Cm     yes no
```

Figure 5
Determining whether transitions corresponding to group–subgroup pairs are according to renormalization group (RG) or Landau theory allowed to be continuous.

[3] The reader intending to follow the detail of our arguments is encouraged to refer to the documentation available at the *ISOTROPY* web site (http://stokes.byu.edu/isotropy.html), in particular the Tutorial.

B-cation displacement could produce a tetragonal structure in space group *P*4*mm*, on a cell essentially the same size as the $Pm\bar{3}m$ cell, then *ISOTROPY* could immediately identify the pertinent irrep as Γ_4^-.

2.3. *B*-cation displacement (antiferroelectric)

An antiferroelectric pattern of *B*-cation displacements is encountered in tungsten trioxide, WO_3. (This is a perovskite missing the *A* cation.) If we consider what would be a (001) plane of W ions in an ideal perovskite structure, the displacements of W ions are perpendicular to this plane and in alternating sense. This leads to a doubling of the repeat distance in both *x* and *y* directions, so we seek an irrep at the *M* point ($\boldsymbol{k} = 1/2, 1/2, 0$) of reciprocal space that produces the required displacements at Wyckoff *a* sites (Fig. 6).

Although there are two irreps producing displacements at Wyckoff *a*, only for M_3^- are the displacement vectors in the [001] direction as required. The displacement is in the positive direction for the ions at (0,0,0) and (0,0,1), and in the negative direction for the ions at (1,0,0) and (0,1,0). Evidently, M_3^- is the irrep required. A further application of *ISOTROPY* shows that irrep M_3^- with order parameter (*a*,0,0) leads to a structure in *P*4/*nmm*, as is observed in WO_3 above 1173 K (Howard *et al.*, 2002).

2.4. BX_6 octahedral tilting

The most commonly occurring distortion in perovskites is octahedral tilting. By this we mean the tilting of the BX_6 octahedra about one or more of their symmetry axes, maintaining both regularity of the octahedra (approximately) and their corner connectivity (strictly). Such tilting allows greater flexibility in the coordination of the *A* cation, while leaving the environment of the *B* cation essentially unchanged. We shall find it is also a major contributor to structural variability in perovskites.

The first systematic analysis of octahedral tilting was undertaken by Glazer (1972, 1975), who developed a description of the different possible patterns of octahedral tilting, then obtained space groups by inspection. Glazer's description was in terms of component tilts around the 'pseudo-cubic' axes, that is the cubic axes of the parent structure. He noted that the tilt of one octahedron around one of these axes determines (*via* the corner connections) the tilts of all the octahedra in the plane perpendicular to this axis, but that successive octahedra along the axis can be tilted in either the same or the opposite sense. The structure of $SrZrO_3$ at 1073 K (Fig. 7) provides a simple example of octahedral tilting. Glazer describes the tilting using symbols of the form $a^{\#}b^{\#}c^{\#}$ in which the literals refer in turn to tilts around axes in the *x*, *y* and *z* directions of the $Pm\bar{3}m$ parent structure. The repetition of a letter indicates that the tilts about the corresponding axes are equal in magnitude. The superscript # takes the value + or − to indicate that the tilts of successive octahedra along the relevant axis are in the same or opposite sense. We use the terms 'in-phase' tilting to describe the former case (+) and 'out-of-phase' tilting for the latter (−). For directions about which there is no octahedral tilting, we show the superscript # as 0. The Glazer symbols for describing octahedral tilting are now almost universally adopted.

The group-theoretical analysis of octahedral tilting was described in a previous paper (Howard & Stokes, 1998), and we must refer the reader to that paper for details. The order parameter is a six-component vector with components proportional to the angles of in-phase and out-of-phase tilting around axes in the *x*, *y* and *z* directions of the parent structure. It is found that none of the operations *g* of $Pm\bar{3}m$ mix in-phase (+) and out-of-phase (−) tilting, so we consider this to comprise two three-component vectors, one for the in-phase tilting and one for the out-of-phase tilting, and each carrying a three-dimensional irrep of the parent space group $Pm\bar{3}m$. To analyse this situation, we can run *ISOTROPY* to show the rotations around a given Wyckoff position ('show microscopic vector pseudo') rather than the vector displacements we have shown before. (Rotations and spins transform like pseudovectors, sometimes also called axial vectors.) We find (see Appendix *A* in Howard & Stokes, 1998, or Case Study 1 in the *ISOTROPY* Tutorial) that the irrep associated with the in-phase tilts is M_3^+ ($\boldsymbol{k} = 1/2, 1/2, 0$) and that associated with the out-of-phase tilts is R_4^+ ($\boldsymbol{k} = 1/2, 1/2, 1/2$). We show, by way of illustration (Fig. 8), the search at the *R* point.

Evidently, R_4^+ is the only *R*-point irrep leading to any tilting of octahedra centred on the Wyckoff positions *a*. Restricting

```
Isotropy, Version 6.4.2, August 2000
Harold T. Stokes and Dorian M. Hatch
Brigham Young University
*DISPLAY SETTING
Current setting is International (new ed.) with conventional basis vectors.
*value parent 221
*value kpoint m
*value wyckoff a
*show irrep
*show microscopic vector
*display distortion
Irrep (ML) Point   Mode Projected Vectors
M3-        (0,0,0) 1    (0,0,1),  (1,0,0),  (0,1,0)
           (1,0,0) 1    (0,0,-1), (1,0,0),  (0,-1,0)
           (0,1,0) 1    (0,0,-1), (-1,0,0), (0,1,0)
           (0,0,1) 1    (0,0,1),  (-1,0,0), (0,-1,0)
M5-        (0,0,0) 1    (1,0,1),   (1,0,-1),  (1,1,0),   (-1,1,0),  (0,1,1),   (0,-1,1)
           (1,0,0) 1    (-1,0,-1), (-1,0,1),  (-1,-1,0), (1,-1,0),  (0,1,1),   (0,-1,1)
           (0,1,0) 1    (1,0,1),   (1,0,-1),  (-1,-1,0), (1,-1,0),  (0,-1,-1), (0,1,-1)
           (0,0,1) 1    (-1,0,-1), (-1,0,1),  (1,1,0),    (-1,1,0), (0,-1,-1), (0,1,-1)
*quit
```

Figure 6
Finding the irrep that gives antiferroelectric *B*-cation displacements.

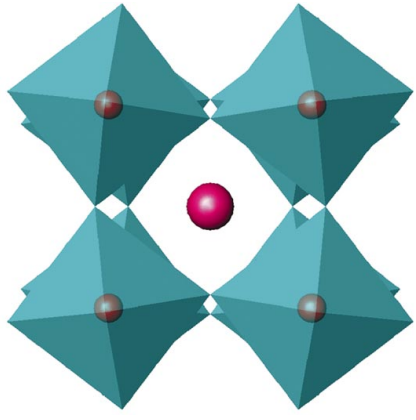

Figure 7
The structure $SrZrO_3$ at 1073 K. The tilting of corner-linked octahedra is evident, as is the fact that the two layers shown tilt in opposite sense. The tilt system in Glazer's notation is $a^0a^0c^-$.

attention to the first of the 'projected pseudo vectors', we see a positive tilt around an axis in the parent z direction for the octahedron centred on 0,0,0, negative tilts as required by corner connectivity of the octahedra at 1,0,0 and 0,1,0, and at 0,0,1 a negative tilt consistent with tilting of successive octahedra along the tilt axis being tilted in the opposite sense (out-of-phase tilting). This confirms that R_4^+ is the required irrep.

The irreps being established, the procedure for finding the isotropy subgroups is similar to that followed in §2.2. Setting the irrep first as M_3^+ leads to a listing of isotropy subgroups corresponding to in-phase tilts alone, and setting it next as R_4^+ lists those corresponding to out-of-phase tilts. Structures involving both in-phase and out-of-phase tilting are listed using instructions 'value irrep M3+ R4+' followed by 'display isotropy coupled'. These instructions produce a list of 14 isotropy subgroups together with the relevant order parameters (see *ISOTROPY* Tutorial, Case Study 1). We exclude ten of these subgroups because they show both in-phase (+) and out-of-phase (−) tilting around the same axis and so do not correspond to 'simple' tilts. By this we mean that the tilts would differ in magnitude (and possibly also in sense) between one octahedron and the next, a circumstance we choose to exclude from our consideration. Group–subgroup relationships are determined from the order parameters in the usual way, and *ISOTROPY* is used to examine each group–subgroup pair to determine whether the corresponding phase transition is allowed to be continuous. The results from our analysis of octahedral tilting in perovskites are summarized here in Fig. 9, reproduced from the erratum by Howard & Stokes (2002).

The analysis of octahedral tilting just described raises a number of matters meriting additional comment:

- The only tilt systems considered are those in which successive octahedra along the tilt axis either all have the same sense of tilt or alternate in sense. More complex patterns of tilting (*e.g.* two octahedra tilting in one sense, the next two in the opposite sense) have been excluded at the outset.
- The problem involves two irreps, M_3^+ and R_4^+, and so provides an example of the combined effect of two distortions.

```
Isotropy, Version 6.4.2, August 2000
Harold T. Stokes and Dorian M. Hatch
Brigham Young University
*DISPLAY SETTING
Current setting is International (new ed.) with conventional basis vectors.
*v parent 221
*v kpoint r
*v wyckoff a
*show irrep
*show microscopic vector pseudo
*value cell 2,0,0 0,2,0 0,0,2
*display distortion
Irrep (ML) Point   Mode Projected Pseudo Vectors
R4+        (0,0,0) 1    (0,0,1), (1,0,0), (0,1,0)
           (0,0,1) 1    (0,0,-1), (-1,0,0), (0,-1,0)
           (0,1,0) 1    (0,0,-1), (-1,0,0), (0,-1,0)
           (0,1,1) 1    (0,0,1), (1,0,0), (0,1,0)
           (1,0,0) 1    (0,0,-1), (-1,0,0), (0,-1,0)
           (1,0,1) 1    (0,0,1), (1,0,0), (0,1,0)
           (1,1,0) 1    (0,0,1), (1,0,0), (0,1,0)
           (1,1,1) 1    (0,0,-1), (-1,0,0), (0,-1,0)
*quit
```

Figure 8
The search at the R point ($\boldsymbol{k} = 1/2, 1/2, 1/2$) for an irrep associated with octahedral tilting. Subsequent application of *ISOTROPY* will yield order parameters with components referring to tilts around axes in z, x and y directions in turn.

ISOTROPY proves particularly powerful when the combined effects of two or more distortions must be considered.

- Only 'simple' tilt systems have been accepted. That is, structures showing non-zero positive and negative tilts around the same axis have been culled from the results.
- We have argued (Howard & Stokes, 1998) that, as regards octahedral tilting, the tilt system within a particular isotropy subgroup will adopt the lowest symmetry consistent with the space-group symmetry. For example, the structure in *Cmcm* allows a tilt system $a^0b^+c^-$ (see Fig. 9), and we have argued that tilt system $a^0b^+b^-$ based on some accidental equality of the in-phase and out-of-phase tilt angles will not in fact occur. By this means, we have reduced Glazer's list of 23 tilt systems to the 15 shown in Fig. 9.

Octahedral tilting occurs in combination with other distortions, such as the ferro- and antiferroelectric patterns of B-cation displacement described in §§2.2 and 2.3. The former case, involving combinations of Γ_4^- with M_3^+ and R_4^+, has been treated by Stokes *et al.* (2002). The results comprise the 7 structures shown in Fig. 2, the 15 structures shown in Fig. 9 (noting however the repetition of the parent structure in $Pm\bar{3}m$), and 40 additional structures with both tilts and B-cation displacements. Glazer's notation was extended to convey information on the cation displacement as well as on tilts. The case of antiferroelectric displacements, involving combinations of M_3^- with M_3^+ and R_4^+ has been considered by Howard *et al.* (2002). Under the condition that the order parameter for M_3^- is $(a,0,0)$, as it is for the high-temperature tetragonal form of WO_3, or of derivative lower symmetry, such as $(a,b,0)$, 18 different structures were found.

2.5. Double perovskites $A_2BB'X_6$ and B-site cation ordering

Substitution of cation B' for B leads in general to the solid solution $AB_{1-x}B'_xX_3$, but if $x \approx 0.5$ and B and B' differ suffi-

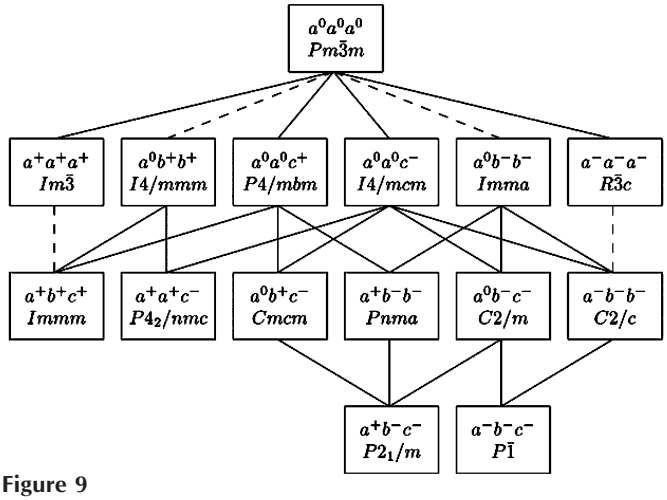

Figure 9
A schematic diagram recording the structures for perovskites found by Howard & Stokes (1998). The diagram shows the space-group symmetry, along with the Glazer (1972) symbol for the tilts. The lines indicate group–subgroup relationships, and a dashed line joining a group with its subgroup means that the corresponding phase transition is in Landau theory required to be first order. The figure has been reproduced from Howard & Stokes [*Acta Cryst.* (2002), B**58**, 565].

ciently in charge and/or size then *B*-site cation ordering may occur. The formula is then properly written as $A_2BB'X_6$ and the compound is described as a double perovskite. The most common ordering that occurs in such compounds is a rock-salt ordering of *B* and *B*′ cations over the parent *B* (Wyckoff *a*) sites.[4] This ordering will lead to a doubling of the unit cell in every direction, and so is expected to be associated with the *R* point ($\boldsymbol{k}$ = 1/2, 1/2, 1/2) of reciprocal space. The search for the irrep proceeds as follows (Fig. 10), showing scalar distortions (in this case atomic occupancy) at the Wyckoff *a* sites.

Taking *f* and −*f* to indicate sites occupied by *B* and *B*′ cations, respectively, it is seen that the one-dimensional irrep R_1^+ is the irrep required. The ordered structure is in space group $Fm\bar{3}m$ on a 2 × 2 × 2 unit cell. The combination of *B*-cation ordering, irrep R_1^+, with octahedral tilting, irreps M_3^+ and R_4^+, represents a straightforward application of *ISOTROPY*, and 12 different structures result (Fig. 11).

In relation to this work (Howard *et al.*, 2003), we mention that:

- There are some differences between the Howard, Kennedy & Woodward results and those published earlier by Aleksandrov & Misyul (1981). The most significant relate to the retention by Aleksandrov & Misyul of structures with both in-phase and out-of-phase tilts around the same axis. Howard, Kennedy & Woodward rejected these on the grounds they were not 'simple' tilts.
- The structure of Sr_2YTaO_6 originally reported as triclinic (Woodward, 1997*c*) has been re-examined and shown to be monoclinic, tilt system $a^-a^-c^+$ in space group $P2_1/n$. Sr_2YNbO_6 adopts the same structure (Howard *et al.*, in preparation)
- The Howard, Kennedy & Woodward review of known structures, if expanded to include the *A*-site-deficient double hydroxides $BB'(OH)_6$ listed by Mitchell (2002), would show examples such as schoenfliesite $MgSn(OH)_6$ in space group $Pn\bar{3}$, mushistonite $CuSn(OH)_6$ in space group $P4_2/nnm$, and stottite $FeGe(OH)_6$ in space group $P4_2/n$. These display symmetries not otherwise encountered in the double perovskites.[5]

Aleksandrov & Misyul (1981) considered combinations of cation ordering, irrep R_1^+, with both ferroelectric patterns of *B*-cation displacement, irrep Γ_4^-, and octahedral tilting, irreps M_3^+ and R_4^+. The application of *ISOTROPY* is again straightforward, although the listings are too long to reproduce here. Along with the 12 tilting-only structures appearing in Fig. 11, we find 6 structures with *B*-cation displacements but no tilting ($R_1^+ \oplus \Gamma_4^-$), 14 structures combining *B*-cation displacements with in-phase tilting ($R_1^+ \oplus \Gamma_4^- \oplus M_3^+$), 6 structures combining *B*-cation displacements with out-of-phase tilting ($R_1^+ \oplus \Gamma_4^- \oplus R_4^+$), and 5 structures with simple tilts (from a list of 14 in total) combining *B*-cation displacements with both in-phase and out-of-phase tilting ($R_1^+ \oplus \Gamma_4^- \oplus M_3^+ \oplus R_4^+$). The interested reader should encounter no difficulty in reproducing these results. The results are summarized in Table 2, where we use the modified Glazer notation (Stokes *et al.*, 2002), subscripts + and − being used to denote ferroelectric *B*-cation displacements along a given axis, and superscripts retaining their usual meaning.

```
Isotropy, Version 6.4.2, August 2000
Harold T. Stokes and Dorian M. Hatch
Brigham Young University
*DISPLAY SETTING
Current setting is International (new ed.) with conventional basis vectors.
*value parent 221
*value kpoint r
*value wyckoff a
*show irrep
*show microscopic scalar
*value cell 2,0,0 0,2,0 0,0,2
*display distortion
Irrep (ML) Point   Mode Projected Order Functions
R1+        (0,0,0) 1    f
           (0,0,1) 1    -f
           (0,1,0) 1    -f
           (0,1,1) 1    f
           (1,0,0) 1    -f
           (1,0,1) 1    f
           (1,1,0) 1    f
           (1,1,1) 1    -f
*value irrep r1+
*cancel show irrep
*show subgroup
*show origin
*display isotropy
Subgroup  Origin
225 Fm-3m (0,0,0)
*quit
```

Figure 10
Finding the irrep that gives rock-salt ordering on the *B* site.

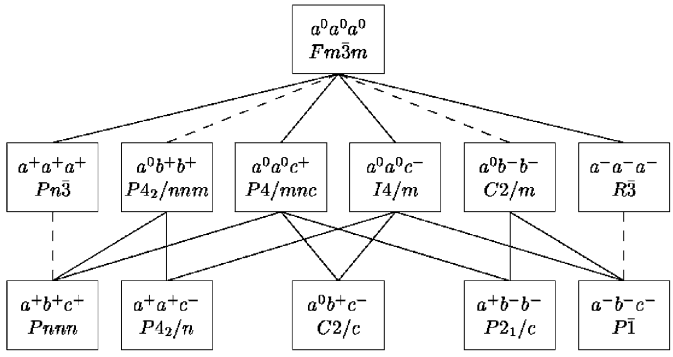

Figure 11
A schematic diagram indicating the group–subgroup relationships among the structures formed by the double perovskites $A_2BB'X_6$ with a rock-salt pattern of *B*-cation ordering. Full details of the structures are to be found in the paper by Howard *et al.* (2003).

```
Isotropy, Version 6.4.2, August 2000
Harold T. Stokes and Dorian M. Hatch
Brigham Young University
*DISPLAY SETTING
Current setting is International (new ed.) with conventional basis vectors.
*value parent pm-3m
*value subgroup im-3m
*show parent
*show subgroup
*show basis
*show origin
*show irrep
*show direction vector
*display isotropy
Parent    Irrep (ML) Subgroup  Dir         Basis Vectors              Origin
221 Pm-3m M1+        229 Im-3m P3  (a,a,a) (2,0,0),(0,2,0),(0,0,2) (0,0,0)
221 Pm-3m M4+        229 Im-3m P3  (a,a,a) (2,0,0),(0,2,0),(0,0,2) (1/2,1/2,1/2)
*quit
```

Figure 12
Finding the irrep that gives a body-centred pattern of 1:3 ordering on the *B* site.

[5] The structures formed, being related to elpasolite K_2NaAlF_6, are referred to as elpasolites.

[5] In fact, Howard *et al.* (2003) recognized certain double perovskites with mixed *A*-site occupancy as examples showing $Pn\bar{3}$ space-group symmetry, but they found no other examples of the structures in space groups $P4_2/nnm$ or $P4_2/n$.

There is a measure of agreement between these results and those of Aleksandrov & Misyul (1981),[6] but a detailed comparison is difficult. Discrepancies arise because Aleksandrov & Misyul retain structures with polarization direction or tilt systems showing higher symmetries than the space group will allow. For example, for tilt system $a^+a^+a^+$ (or $\psi\psi\psi$ in their notation), we find the only polar structure is (using modified Glazer symbols) $a^+_+a^+_+a^+_+$ in $R3$. Aleksandrov & Misyul evidently record structures in $Pnn2$ for $\psi\psi\psi/00p$ (their reference), and in Pc for $\psi\psi\psi/pp0$. We find these structures are respectively $a^+_0b^+_0c^+_+$ and $a^+_+b^+_+c^+_0$. Both structures allow the three tilt angles to be different, and the second of these also allows the two non-zero polarization components to differ. We do not expect to find a structure with equal tilt angles in either space group $Pnn2$ or Pc, nor one with polarization components equal in Pc. In addition, we find errors in some space-group symmetries, such as for systems [reference in Aleksandrov & Misyul's (1981) tables given in parentheses] $a^0_+a^0_+c^+_+$ $(00\psi/p_1p_1p_2)$, $a^0_0b^+_0c^-_0$ $(\psi0\phi/00p)$ and $a^0_+b^+_+c^-_0$ $(\psi0\phi/p_1p_20)$.

2.6. Perovskites $A_4BB'_3X_{12}$ – 1:3 *B*-site cation ordering

We refer here to a body-centred pattern of ordering on the perovskite B sites. This cation arrangement is found, for example, in $Ba_4LiSb_3O_{12}$, which is cubic in space group $Im\bar{3}m$ on a $2 \times 2 \times 2$ unit cell (Jacobson *et al.*, 1974). In this case, we will find the irrep using our knowledge of the parent structure in $Pm\bar{3}m$ and the derived $Im\bar{3}m$ structure.

This search (Fig. 12) produces two candidate irreps. Given that the structure in $Im\bar{3}m$ is on the same origin as the parent structure in$Pm\bar{3}m$, it is clear that M^+_1 is the appropriate irrep,[7] the order parameter being (a,a,a). This result can be checked using 'display distortions'.

The combination of this cation ordering, irrep M^+_1, with octahedral tilting, irreps M^+_3 and R^+_4, has been examined recently by Howard & Stokes (2004). The analysis involves additional arguments specific to the case of cation ordering associated with multidimensional irreps (in contrast to the cation ordering of §2.5 where the irrep was one-dimensional). We illustrate with the results obtained from the combination of the cation ordering M^+_1 with in-phase octahedral tilting M^+_3 (Fig. 13).

Now the first three components of the order parameter relate to the cation ordering M^+_1, and the last three to the in-phase octahedral tilting M^+_3. The last three components correspond in fact to tilts around axes in the z, x and y directions, respectively, of the parent structure (see Fig. 8; also Appendix A in Howard & Stokes, 1998, and Case Study 1, *ISOTROPY* Tutorial). What we see is that only one of the listed subgroups, $R\bar{3}$, tilt system $a^+a^+a^+$, shows the full symmetry (a,a,a) of the cation ordering. The argument here is that we must accept certain of the structures allowing but not requiring a cation arrangement with order parameter (a,a,a) – that is with M^+_1 order parameters (a,a,b) or (a,b,c). The structures we accept are those, such as that in $I4/m$, tilt system $a^0a^0c^+$, where it is the tilting that forces the lower space-group symmetry. The space-group symmetry allows but does not require a cation arrangement of a lower symmetry than the 1:3 arrangement we suppose. The structures we reject include those such as that in $C2/m$, order parameter $(a,b,c,d,0,0)$, same tilt system and a subgroup of $I4/m$, where the further

Table 2
Isotropy subgroups of $Pm\bar{3}m$ for the irrep R^+_1 in combination with irreps Γ^-_4 and/or M^+_3 and/or R^+_4.

For each subgroup, we show the space-group symmetry (number), the order parameters for the irreps involved, and the tilt-displacement system in a modified Glazer (1972, 1975) notation. The components of the order parameter associated with Γ^-_4 indicate B-cation displacements in the x, y, z directions (of the parent structure), respectively, and the components of the order parameters associated with irreps M^+_3 and R^+_4 have been permuted to show tilts around the axes in the x, y, z directions. Lattice vectors and origins for the isotropy subgroups can be obtained from *ISOTROPY* as required. It will be found, for example, that structures in systems $a^0_+b^0_+c^0_0$ and $a^0_+a^0_+c^0_+$, both in space group Cm, are on different cells.

Space group	Γ^-_4	M^+_3	R^+_4	System
$Fm\bar{3}m$ (No. 225)	(0,0,0)	(0,0,0)	(0,0,0)	$a^0_0a^0_0a^0_0$
$I4mm$ (No. 107)	(0,0,a)	(0,0,0)	(0,0,0)	$a^0_0a^0_0c^0_+$
$Imm2$ (No. 44)	(a,a,0)	(0,0,0)	(0,0,0)	$a^0_+a^0_+c^0_0$
$R3m$ (No. 160)	(a,a,a)	(0,0,0)	(0,0,0)	$a^0_+a^0_+a^0_+$
Cm (No. 8)	(a,b,0)	(0,0,0)	(0,0,0)	$a^0_+b^0_+c^0_0$
Cm (No. 8)	(a,a,b)	(0,0,0)	(0,0,0)	$a^0_+a^0_+c^0_+$
$P1$ (No. 1)	(a,b,c)	(0,0,0)	(0,0,0)	$a^0_+b^0_+c^0_+$
$P4/mnc$ (No. 128)	(0,0,0)	(0,0,a)	(0,0,0)	$a^0_0a^0_0c^+_+$
$Ama2$ (No. 40)	(a,0,0)	(0,0,b)	(0,0,0)	$a^0_+b^0_0c^+_+$
$P4nc$ (No. 104)	(0,0,a)	(0,0,b)	(0,0,0)	$a^0_0a^0_0c^+_+$
$Pmn2_1$ (No. 31)	(a,a,0)	(0,0,b)	(0,0,0)	$a^0_+a^0_+c^+_0$
Pm (No. 6)	(a,b,0)	(0,0,c)	(0,0,0)	$a^0_+b^0_+c^+_0$
Cc (No. 9)	(a,0,b)	(0,0,c)	(0,0,0)	$a^0_+b^0_0c^+_+$
Pc (No. 7)	(a,a,b)	(0,0,c)	(0,0,0)	$a^0_+a^0_+c^+_+$
$P1$ (No. 1)	(a,b,c)	(0,0,d)	(0,0,0)	$a^0_+b^0_+c^+_+$
$P4_2/nnm$ (No. 134)	(0,0,0)	(0,a,a)	(0,0,0)	$a^0_0b^+_0b^+_0$
$P4_2nm$ (No. 102)	(a,0,0)	(0,b,b)	(0,0,0)	$a^0_+b^+_0b^+_0$
$Abm2$ (No. 39)	(0,a,a)	(0,b,b)	(0,0,0)	$a^0_0b^+_+b^+_+$
Cm (No. 8)	(a,b,b)	(0,c,c)	(0,0,0)	$a^0_+b^+_+b^+_+$
$Pn\bar{3}$ (No. 201)	(0,0,0)	(a,a,a)	(0,0,0)	$a^+_0a^+_0a^+_0$
$R3$ (No. 146)	(a,a,a)	(b,b,b)	(0,0,0)	$a^+_+a^+_+a^+_+$
$Pnnn$ (No. 48)	(0,0,0)	(a,b,c)	(0,0,0)	$a^+_0b^+_0c^+_0$
$Pnn2$ (No. 34)	(0,0,a)	(b,c,d)	(0,0,0)	$a^+_0b^+_0c^+_+$
Pc (No. 7)	(a,b,0)	(c,d,e)	(0,0,0)	$a^+_+b^+_+c^+_0$
$P1$ (No. 1)	(a,b,c)	(d,e,f)	(0,0,0)	$a^+_+b^+_+c^+_+$
$I4/m$ (No. 87)	(0,0,0)	(0,0,0)	(0,0,a)	$a^0_0a^0_0c^-_0$
$I4$ (No.79)	(0,0,a)	(0,0,0)	(0,0,b)	$a^0_0a^0_0c^-_+$
Cm (No. 8)	(a,b,0)	(0,0,0)	(0,0,c)	$a^0_+b^0_+c^-_0$
$C2/m$ (No. 12)	(0,0,0)	(0,0,0)	(0,a,a)	$a^0_0b^-_0b^-_0$
$C2$ (No. 5)	(0,a,a)	(0,0,0)	(0,b,b)	$a^0_0b^-_+b^-_+$
Cm (No. 8)	(a,b,b)	(0,0,0)	(0,c,c)	$a^0_+b^-_+b^-_+$
$R\bar{3}$ (No. 148)	(0,0,0)	(0,0,0)	(a,a,a)	$a^-_0a^-_0a^-_0$
$R3$ (No. 146)	(a,a,a)	(0,0,0)	(b,b,b)	$a^-_+a^-_+a^-_+$
$P\bar{1}$ (No. 2)	(a,b,c)	(0,0,0)	(0,0,0)	$a^-_0b^-_0c^-_0$
$P1$ (No. 1)	(a,b,c)	(0,0,0)	(d,e,f)	$a^-_+b^-_+c^-_+$
$C2/c$ (No. 15)	(0,0,0)	(0,a,0)	(0,0,b)	$a^0_0b^0_0c^-_0$
$C2$ (No. 5)	(0,0,a)	(0,b,0)	(0,0,c)	$a^0_0b^+_0c^-_+$
Cc (No. 9)	(a,b,0)	(0,c,0)	(0,0,d)	$a^0_+b^+_+c^-_0$
$P2_1/c$ (No. #14)	(0,0,0)	(a,0,0)	(0,b,b)	$a^+_0b^-_0b^-_0$
$P2_1$ (No. 4)	(0,a,a)	(b,0,0)	(0,c,c)	$a^+_0b^-_+b^-_+$
Pc (No. 7)	(a,b,b)	(c,0,0)	(0,d,d)	$a^+_+b^-_+b^-_+$
$P4_2/n$ (No. 86)	(0,0,0)	(a,a,0)	(0,0,b)	$a^+_0a^+_0c^-_0$
$P4_2$ (No. 77)	(0,0,a)	(b,b,0)	(0,0,c)	$a^+_0a^+_0c^-_+$

[7] The results are reproduced by Aleksandrov & Bartolomé (2001) as their Table VII. There is a typographical error in this table, in that the heading $p_1p_1p_2$ has been transcribed as $p_1p_2p_3$.
[7] The alternate irrep M^+_4 gives an ordering pattern on the A-cation (Wyckoff b) sites.

reduction of symmetry would be a consequence of the lower cation symmetry alone. Applying these arguments, we have, for the combination of M_1^+ cation ordering and in-phase octahedral tilting M_3^+, structures in $R\bar{3}$ ($a^+a^+a^+$), $I4/m$ ($a^0a^0c^+$), $C2/m$ ($a^0b^+b^+$) and $P\bar{1}$ ($a^+b^+c^+$). The reader is referred to Howard & Stokes (2004) for the full results.

The argument here contrasts with that advanced when considering octahedral tilts. In the case of tilts, we argued (§2.4) that the order parameter will always show the lowest symmetry that the space group will allow. For the cation ordering considered here, we argue that the symmetry may very well remain higher than the space-group symmetry will allow. The difference relates to the different mechanisms involved – it is envisaged that octahedral tilting is very readily and quickly accommodated, whereas cation rearrangement is a diffusion-controlled process expected to be extremely slow under normal conditions.

2.7. Perovskites $A_3BB'_2X_9$ – 1:2 *B*-site cation ordering

A number of perovskites, for example $Ba_3ZnTa_2O_9$, show a layering of different *B*-site cations onto (111) planes of the parent perovskite, one layer of *B* cations being followed by two layers of *B′* cations (Galasso & Pyle, 1963). The cation ordering in this case is evidently associated with the point $\boldsymbol{k}$ = 1/3, 1/3, 1/3 of reciprocal space, that is the point on the Λ line α, α, α where $\alpha = 1/3$. This perovskite has, in the absence of octahedral tilting, a structure in space group $P\bar{3}m1$ (Jacobson *et al.*, 1976). First, using *ISOTROPY*, we find that the irreps on the Λ line are Λ_1, Λ_2, Λ_3. Then we examine these irreps in turn, setting $\alpha = 1/3$ in each case (Fig. 14).

Evidently, the eight-dimensional Λ_1 ($\boldsymbol{k}$ = 1/3, 1/3, 1/3) is the irrep to be associated with this pattern of cation ordering, the order parameter being $(a, 0, 0, 0, 0, 0, 0, 0)$.

The combination of this 1:2 cation ordering, irrep Λ_1, with octahedral tilting, irreps M_3^+ and R_4^+, has also been examined by Howard & Stokes (2004). It might have been expected that the eight-dimensional irrep Λ_1 would pose problems similar to those encountered in the case of the three-dimensional irrep M_1^+ (§2.6), but such was not the case. There were, among those structures not requiring the order parameter to be $(a,0,0,0,0,0,0,0)$, no additional tilt systems to be found. In summary, ten different structures were found, and the group–subgroup relationships determined. Full details can be found in Howard & Stokes (2004).

The analysis of these 1:2 perovskites uncovered one final complication. Whereas in all previous work the symbol $a^-a^-c^0$ could be used to describe octahedral tilting around either [110] or [1$\bar{1}$0], in the 1:2 perovskites, these are not equivalent. This is because the layered ordering, irrep Λ_1 order parameter $(a, 0, 0, 0, 0, 0, 0, 0)$, makes the [111] direction unique. Distinct tilt symbols, such as $a^-a^-c^0$ and $a^-\bar{a}^-c^0$, are needed to distinguish the different possibilities. More on this matter can be found in Howard & Stokes (2004).

2.8. A summary of the group-theoretical procedures

The first step is to associate with each of the distortions to be considered an irreducible representation (irrep) of the parent space group $Pm\bar{3}m$. As can be seen above, we use *ISOTROPY* to help in this step. A number of results, including those given above, are summarized in Table 3.

The structures produced by these different distortions (irreps), acting separately or in combination, can be enumerated quite readily by a further application of *ISOTROPY*. The different structures are described by different values of some (generally vector) order parameters, with component(s) representing the magnitude(s) of the distortion(s) present. A particular value of the order parameter corresponds to a particular distorted structure, and the space-group symmetry of that structure is defined by the isotropy subgroup, comprising the operations of the parent space group that leave this order parameter unchanged. For any irrep or combination of irreps, *ISOTROPY* lists all the isotropy subgroups, along with values of order parameter that describe the structures involved. In some cases and after careful examination, certain of the structures listed by *ISOTROPY* are rejected. For example, in considering octahedral tilting, we removed those structures showing both in-phase and out-of-phase tilts around

```
  Isotropy, Version 6.4.2, August 2000
Harold T. Stokes and Dorian M. Hatch
Brigham Young University
*DISPLAY SETTING
Current setting is International (new ed.) with conventional basis vectors.
*value parent 221
*value irrep m1+ m3+
*show subgroup
*show direction vector
*show basis
*show origin
*display isotropy coupled
Subgroup Dir                    Basis Vectors                 Origin
83 P4/m  P1(1)P1(1) (a,0,0,b,0,0) (1,1,0),(-1,1,0),(0,0,1)     (0,0,0)
74 Imma  P1(1)P1(2) (a,0,0,0,0,b) (0,2,0),(0,0,2),(2,0,0)      (0,0,0)
87 I4/m  C2(1)P1(2) (a,a,b,0,0,c) (2,0,0),(0,0,-2),(0,2,0)     (0,0,0)
12 C2/m  S1(1)P1(1) (a,b,c,d,0,0) (2,-2,0),(0,0,2),(0,-2,0)    (0,0,0)
148 R-3  P3(1)P3(1) (a,a,a,b,b,b) (-2,2,0),(2,0,-2),(-1,-1,-1) (0,0,0)
69 Fmmm  P1(1)P2(3) (a,0,0,0,0,b,b) (0,0,-2),(2,2,0),(2,-2,0)    (1/2,-1/2,-1/2)
12 C2/m  C2(1)P2(1) (a,a,b,c,c,0) (0,-2,0),(2,0,2),(-1,1,1)    (0,0,0)
12 C2/m  P1(1)S1(1) (a,0,0,b,c,d) (2,-2,0),(0,0,2),(0,-2,0)    (1/2,-1/2,1/2)
2 P-1    S1(1)S1(1) (a,b,c,d,e,f) (1,1,1),(1,1,-1),(-1,1,1)    (0,0,0)
*quit
```

Figure 13
Listing isotropy subgroups for a perovskite with both 1:3 cation ordering (irrep M_1^+) and in-phase octahedral tilting (irrep M_3^+).

```
Isotropy, Version 6.4.2, August 2000
Harold T. Stokes and Dorian M. Hatch
Brigham Young University
*DISPLAY SETTING
Current setting is International (new ed.) with conventional basis vectors.
*value parent pm-3m
*value subgroup p-3m1
*value irrep ld1
*value kvalue 1,1/3
*show subgroup
*show basis
*show origin
*show irrep
*show direction vector
*display isotropy
Irrep (ML) Subgroup  Dir                    Basis Vectors                 Origin
LD1        164 P-3m1 P1  (a,0,0,0,0,0,0,0) (-1,1,0),(1,0,-1),(-1,-1,-1) (0,0,0)
*value irrep ld2
*value kvalue 1,1/3
*display isotropy
*value irrep ld3
*value kvalue 1,1/3
*display isotropy
*quit
```

Figure 14
Finding the irrep corresponding to the 1:2 *B*-site cation ordering found for example in $Ba_3ZnTa_2O_9$. The work is facilitated by knowing the structure resulting from the cation ordering alone. Note the need to check all irreps on the Λ line to confirm that only one of these gives a structure in the specified space group.

Table 3
Irreducible representations (irreps) of $Pm\bar{3}m$ associated with distortions in perovskites.

Distortion	Irrep	Example
Octahedral distortions (Jahn–Teller)	R_4^+	$KCuF_3$
B-cation displacement (ferroelectric)	Γ_4^-	$BaTiO_3$ (300 K)
B-cation displacement (antiferroelectric)	M_3^-	WO_3 (1000 K)
BX_6 octahedral tilting (in-phase)	M_3^+	$NaTaO_3$ (843 K)
BX_6 octahedral tilting (out-of-phase)	R_4^+	$SrTiO_3$ (<105 K)
$A_2BB'X_6$ (rock-salt ordering on *B* sites)	R_1^+	Ba_2CaWO_6
$AA'B_2X_6$ (layering on *A* sites)	X_3^-	$LaLa_{1/3}Ti_2O_6$
$A_4BB'_3X_{12}$ (1:3 *B*-site cation ordering)	M_1^+	$Ba_4LiSb_3O_{12}$
$A_3BB'_2X_9$ (1:2 *B*-site cation ordering)	Λ_1 (α = 1/3)	$Ba_3ZnTa_2O_9$

the same axis. In the case of perovskites with 1:3 *B*-site cation ordering, we rejected structures with patterns of cation ordering inconsistent with that assumed.

Group–subgroup relationships, if of interest, can be obtained by inspection of the order parameters. To reiterate, if the subspace spanned by a particular order parameter has higher dimension than that spanned by another order parameter, but includes the latter subspace, the isotropy subgroup associated with the second order parameter is a subgroup of that associated with the first order parameter. Once group–subgroup relationships have been identified, *ISOTROPY* can be used to examine each group–subgroup pair to determine whether the corresponding phase transition is allowed to be continuous.

3. Comparison with previous analyses

The approach we have outlined is very much dependent on the implementation of group theory in the computer program *ISOTROPY*.

As mentioned earlier, the first systematic analysis of octahedral tilting in perovskites ABX_3 was carried out by Glazer (1972). After developing his systematic description, he modelled the different tilt systems and obtained the appropriate space groups by inspection. Glazer listed 23 different tilt systems, and worked out the space group for each. In his enumeration of tilt systems, he distinguished (for example) tilt systems $a^0b^+b^-$ and $a^0b^+c^-$, both belonging to the same *Cmcm* isotropy subgroup. We have argued that, since the space-group symmetry does not require the tilt angles around the *y* and *z* axes to be equal in magnitude (the first is an in-phase and the second an out-of-phase tilt), the first of these tilt systems will not occur. Glazer showed eight tilt systems with higher symmetry, in the sense just described, than required by the corresponding space group. Removing these eight leaves fifteen tilt systems, just the number found in our work (Fig. 9). We found tilt system $a^+a^+c^-$, which Glazer had in *Pmmn*, to have the higher symmetry $P4_2/nmc$, and we rejected the other systems in *Pmmn* on the grounds that the tilts involved were not simple, that is there were + and − tilts around the same axis. The reader is referred to our earlier paper (Howard & Stokes, 1998) for a detailed comparison of our results with Glazer's. Glazer's results have formed the starting point for the analysis of structures showing cation ordering. In his analysis of $A_2BB'X_6$ double perovskites, Woodward (1997*a*) examined each of Glazer's tilt systems, to see which symmetry elements would be destroyed by the R_1^+ cation ordering, and thence to determine the space group. In following Glazer, Woodward listed all 23 tilt systems, conforming to 13 different space groups, one of which derived from the rejected space group *Pmmn*. We found 12 distinct structures in our work (Fig. 11, also Howard *et al.*, 2003). Nagai *et al.* (1997) also based their analysis of perovskites with 1:2 ($\Lambda_1, \alpha = 1/3$) *B*-site cation ordering on Glazer's work, in that these authors determined the space-group symmetry from those elements common to Glazer's tilt system and the cation ordering in question. Again there are some differences, with regard to both space groups and allowed tilt systems, between our results (Howard & Stokes, 2004) and those of Nagai *et al.* In the case of $A_4BB'_3X_{12}$ perovskites with 1:3 (M_1^+) *B*-site cation ordering, Alonso *et al.* (1990) considered the impact of cation ordering on the space group for the common tilt system $a^-a^-c^+$.

Aleksandrov and his co-workers (Aleksandrov, 1976, 1978; Aleksandrov & Misyul, 1981; Aleksandrov & Bartolomé, 2001) have made a substantial contribution to the crystallography of perovskites, and the last mentioned paper presents an excellent and comprehensive review. In his work on ABX_3 perovskites with octahedral tilting, Aleksandrov (1976) identified as we did the irreps of $Pm\bar{3}m$ corresponding to in-phase and out-of-phase octahedral tilting, and listed the possible structures, evidently making use of earlier compilations. It is regrettable that, in our own study of octahedral tilting in ABX_3 perovskites (Howard & Stokes, 1998), we overlooked this early work. Aleksandrov & Bartolomé (2001), however, compared the structures from Howard & Stokes (1998) with those listed earlier by Aleksandrov (1976). After correcting Aleksandrov's space group for the $a^+a^+c^-$ tilt system from *Pmmm* to $P4_2/nmc$, they found the only remaining differences could be attributed to our rejection (§2.4) of tilt systems with higher symmetry than the space group will allow, and of tilt systems showing + and − tilts around the same axis. There is not such good agreement on diagrams showing group–subgroup relationships (Fig. 9) and possible transition paths. We contend that the tendency on lowering temperature is not to increase the number of tilt components *per se* but simply to transform to a lower isotropy subgroup. In a subsequent study, Aleksandrov (1978) examined how the symmetries of the different tilt systems would be lowered by ferroelectric and antiferroelectric patterns of *B*-cation displacements. The results have been corrected and extended (to more general displacement directions) by Aleksandrov & Bartolomé (2001). There are a significant number of discrepancies between the results from our computer-assisted analysis of ferroelectric perovskites and Aleksandrov's results in either original or corrected form. As regards antiferroelectric patterns of *B*-cation displacement, it is not easy to relate the results as presented by Aleksandrov & Bartolomé (2001) to our results for WO_3 (Howard *et al.*, 2002), in part because the former do not encompass more general directions of cation displacement,

such as described by M_3^- order parameter $(a,b,0)$. Aleksandrov & Misyul (1981) also examined the effects of octahedral tilting in the double perovskites $A_2BB'X_6$. They based the analysis on the parent elpasolite in $Fm\bar{3}m$, and found irreps X_3^+ and Γ_4^+ to correspond respectively with in-phase and out-of-phase tilting. As mentioned earlier (§2.5), there are some differences between their results[8] and ours (Howard *et al.*, 2003), which are now largely understood. Aleksandrov & Misyul (1981) proceeded to record how the symmetries of the different structures are reduced by a ferroelectric pattern of *B*-cation displacements, work revisited in §2.5 here.

In another approach to perovskite crystallography, Bärnighausen (1975) has recorded a hierarchy of space groups adopted by the different variants. There being no reference to irreps, it is not clear how any connection may be made to the physical distortions involved. The hierarchy also involves intermediates of no physical significance. For the example of ferroelectric *B*-cation displacement (§2.2), we have argued that displacement of the *B* cation along the *z* axis lowers the symmetry directly from $Pm\bar{3}m$ to $P4mm$. By contrast, Bärnighausen's scheme shows an intermediate space group $P4/mmm$. Bärnighausen's approach has been followed by Bock & Müller (2002). With reference to the double perovskites $A_2BB'X_6$, we have found very significant differences between our results (Howard *et al.*, 2003) and those obtained by Bock & Müller.

A new account of 'tilting structures in perovskites' has been published very recently by Shirokov & Torgashev (2004). These authors, too, use group-theoretical methods in their work. However, they make two assumptions that distinguish their work from that of other authors. First, from among the different structures they obtain, they retain only those structures in which all the *B* sites remain crystallographically equivalent. Secondly, and perhaps more controversially, they allow distortions associated with the six-dimensional irreps X_5^+ and M_5^+ that in our analysis (*ISOTROPY* Tutorial, Case Study 1) were rejected, on the grounds they did not accord with the view of perovskites as containing a three-dimensional network of (nearly) regular corner-linked BX_6 octahedra. The fundamental distortion associated with M_5^+, for example, leaves the four (equatorial) anions of the BX_6 octahedron in their starting plane while moving the two (apical) anions so that the line joining them is no longer perpendicular to the plane of the equatorial anions. This is by no means simply a tilt, and indeed we believe such a distortion is unlikely to occur.[9] In any case, these are not the tilts envisaged by Glazer (1972, 1975), and when such distortions are active we suggest that the Glazer notation should not be employed.

[10] Note that in Table VI of Aleksandrov & Bartolomé (2001), space group C_{3i}^2 ($R\bar{3}$) is shown incorrectly as $R\bar{3}c$.

[9] It should be noted that octahedral distortion is allowed in structures based on irreps M_3^+ and R_4^+, but the tilting does not depend on the octahedral distortion itself.

4. Experimental studies

Following general remarks on the approach to structure determination in perovskites, a selection of experimental studies will be reviewed.

4.1. General remarks

As stated at the outset, distortions in perovskites (Table 3) are often subtle, in which case the structure of the perovskite variant differs little from the parent structure in $Pm\bar{3}m$. The diffraction pattern from the variant then may differ from that from the parent only by a slight broadening or splitting of the main peaks, and the appearance of weak superlattice peaks. It has become our practice to index the main peaks (even if they show splitting) on the basic perovskite cell,[10] and then to assign fractional indices to the superlattice peaks. A definitive structure solution will very likely depend on further knowledge of the perovskite under study, for example whether it is ferroelectric, or a simple ABX_3 perovskite with only octahedral tilting expected, or a double perovskite $A_2BB'X_6$. In such cases, the possibilities can be restricted to those appearing in Figs. 2, 9, or 11, respectively.

Diffraction peak splitting may help to establish the symmetry of the variant under study. For example, tetragonal symmetry is expected to lead to doublet splitting of the *h*00-type reflections while leaving the *hhh*-type reflections as singlets. Rhombohedral symmetry is expected to lead to the reverse effect. More complex patterns of peak splitting very likely indicate orthorhombic or monoclinic symmetry. The best techniques to establish these peak splittings, and so obtain an indication of symmetry, are high-resolution X-ray and neutron powder diffraction. Though peak splittings may help to establish the symmetry, their absence does not prove a higher symmetry, since the symmetry of the metric in perovskites is sometimes higher than the space group will allow. This was the case for $Ca_{0.5}Sr_{0.5}TiO_3$, found to be metrically tetragonal even at the resolution of a good synchrotron-based powder diffractometer (Ball *et al.*, 1998), yet definitely orthorhombic in space group *Pnma* (Howard *et al.*, 2001).

The superlattice peaks will index according to the $\boldsymbol{k}$ value of the relevant irrep. Distortions at the Γ point ($\boldsymbol{k}$ = 0, 0, 0) will produce no additional peaks, but will impact on the intensities of the main perovskite peaks. Distortions at the *X* point ($\boldsymbol{k}$ = 0, 0, 1/2), *M* point ($\boldsymbol{k}$ = 1/2, 1/2, 0), and *R* point ($\boldsymbol{k}$ = 1/2, 1/2, 1/2) will give rise to superlattice peaks indexing with one index half-integral, two indices half-integral, and all indices half-integral, respectively. Perovskites $A_3BB'_2X_9$ with 1:2 cation ordering on the *B* site, irrep at Λ point ($\boldsymbol{k}$ = 1/3, 1/3, 1/3), will give rise to peaks indexing at third-integral values. In electron diffraction parlance (Howard *et al.*, 2001; Ting *et al.*, 2004), with peaks of the parent perovskite at $\mathbf{G}_p$, distortions associated with irreps at the *X*, *M* or *R* point and Λ point (α = 1/3) will give rise to superlattice reflections

[10] This is how we indexed in studies of $SrZrO_3$ (Howard, Knight *et al.*, 2000) and WO_3 (Howard *et al.*, 2002). We have on occasions found it convenient to index on a 2 × 2 × 2 cell (Howard & Zhang, 2003).

at $\mathbf{G}_p \pm 1/2\langle 001\rangle_p$, $\mathbf{G}_p \pm 1/2\langle 110\rangle_p$, $\mathbf{G}_p \pm 1/2\langle 111\rangle_p$ and $\mathbf{G}_p \pm 1/3\langle 111\rangle_p$, respectively. Though we can for any distortion indicate where the superlattice peaks might be found, it is evident from Table 3 that in general we cannot determine distortions unambiguously. That table shows three different distortions at both *M* and *R* points. In addition, the coupling of distortions at different points of reciprocal space can give rise to distortions producing intensity at the sum or difference points – for example the simultaneous presence of *M*- and *R*-point octahedral tilting will produce weaker intensity at the *X* points (Glazer, 1975). This underlines the need for additional information about the distortions involved.

In the event that two distortions operate at the same point of reciprocal space, such as in double perovskites $A_2BB'X_6$ showing both rock-salt cation ordering (R_1^+) and out-of-phase octahedral tilting (R_4^+), the use of more than one diffraction probe is desirable. In double perovskites of typical heavy-metal oxide composition, a combination of X-ray diffraction, which is generally more sensitive to the cation ordering, and neutron diffraction, sensitive to the oxygen movement from octahedral tilting, provides the best means to establish and quantify the extent of cation ordering and the tilts. The particular challenge of these double perovskites has been discussed in greater detail elsewhere (Howard *et al.*, 2003). Electron diffraction has the sensitivity to show the superlattice reflections whenever they occur (Ting *et al.*, 2004), and because of this provides a powerful tool for space-group determination, but considerable care must be exercised to ensure that multiple diffraction effects are avoided (or at least identified) and that samples selected are single domain.[11] In the event that single-crystal diffraction patterns can be recorded (from a single domain), the information on space-group symmetry goes beyond the identification of superlattice spots at the *M* and *R* points. In the electron diffraction investigation of $Ca_{0.5}Sr_{0.5}TiO_3$ mentioned above (Howard *et al.*, 2001), it was possible to distinguish space group *Pnma* from *Cmcm*, even though the corresponding tilt systems both show in-phase (M_3^+) and out-of-phase (R_4^+) tilts (see Fig. 9 and Table 3).

A strategy employed on a number of occasions has been to study the structures as a function of temperature (in fine steps) or composition. A comparison with the sequences suggested in figures such as Figs. 2, 9 or 11 can provide corroborating evidence on the structures involved. Details on the structural phase transitions are also recorded. By means of temperature studies, it has been possible to resolve structural ambiguities in $SrZrO_3$ (Howard, Knight *et al.*, 2000) and WO_3 (Howard *et al.*, 2002). Detailed studies on $PrAlO_3$ (Carpenter *et al.*, 2005) have been completed. A study of the system $SrTiO_3$–$La_{2/3}TiO_3$ as a function of composition and temperature has also been carried out (Howard *et al.*, 2004). It is our experience that phase transitions allowed to be continuous are usually continuous or nearly so, and that transitions required to be first order, either because there is no group–subgroup relationship or by Landau theory, are distinctly discontinuous. From Fig. 9 and space groups *Pnma* and *Cmcm*, it is likely that now we would rule out space group *Cmcm* for $Ca_{0.5}Sr_{0.5}TiO_3$ on the basis that the structure appeared to derive continuously (Ball *et al.*, 1998) from a structure known to be in *Pnma*.

4.2. Barium titanate ($BaTiO_3$)

This is a classic ferroelectric material, discovered during World War II (ch. 4 in Megaw, 1957), and its structures were determined shortly afterwards (Kay & Vousden, 1949). The structure is rhombohedral in *R*3*m* below about 193 K, then orthorhombic in *Amm*2 to 278 K, tetragonal in *P*4*mm* to 393 K, and finally cubic in $Pm\bar{3}m$. It can be seen in Fig. 2 that the first two transitions do not involve group–subgroup pairs, and so must be discontinuous. The transition from tetragonal to cubic, though it is allowed to be continuous, is also first order. There are no superlattice peaks since the distortions are at the Γ point, but in the powder diffraction patterns the splitting of the main peaks is readily observable (ch. 5 in Megaw, 1957; Darlington *et al.*, 1994). Non-centrosymmetric space groups were chosen for the lower-symmetry phases, based on the observations of piezoelectricity in these phases. The fact that the distortions do not produce superlattice peaks, but simply have some effect on the main peak intensities, has made these distortions quite difficult to quantify. Neutron diffraction measurements were made on single crystals, electric fields of 10 kV m^{-1} being applied to these crystals to maintain them as predominantly single domain (Frazer *et al.*, 1955; Shirane *et al.*, 1957). The details of the low-temperature *R*3*m* structure were determined by refinement from neutron powder diffraction data (Hewat, 1974). More recently, Darlington *et al.* (1994) have used the high-resolution powder diffractometer at the ISIS neutron facility (Ibberson *et al.*, 1992) to study $BaTiO_3$ between 150 and 425 K at 5 K intervals of temperature. The symmetry changes were easily detected, and at every temperature the lattice parameters were recorded. Atomic coordinates were also obtained. The rhombohedral and orthorhombic phases were found to coexist at temperatures near 210 K; likewise, the orthorhombic and tetragonal phases co-existed at around 295 K. No two-phase mixtures were observed at the tetragonal-to-cubic phase transition. Although the lattice parameters changed discontinuously at each of the phase transitions, the cell volume varied practically continuously over the whole temperature range. The polarization changes direction at each of these phase transitions (see order parameters in Table 1) but, interestingly, its magnitude (calculated from the atomic coordinates) is little affected by the sudden change in direction. Darlington & Knight (1994) have carried out a very similar study of the structures and phase transitions in $KNbO_3$.

4.3. Strontium zirconate ($SrZrO_3$)

Strontium zirconate is a perovskite showing three temperature-induced phase transitions, but octahedral tilting is considered to be the only distortion involved. Hence the

[11] Standard X-ray and neutron single-crystal techniques are generally not applicable because of the propensity of perovskite variants to form multidomain crystals. The small probe size in electron diffraction offers the possibility of locating single domains.

schematic of Fig. 9 should apply. Carlsson (1967) was the first to examine these transitions, using both X-ray and thermal methods. He summarized his observations in the schematic:

$$\text{orthorhombic} \xrightarrow[\text{continuous}]{973\,K} \underset{c/a<1}{\text{pseudo-tetragonal}} \xrightarrow[\text{discontinuous}]{1103\,K} \underset{c/a>1}{\text{tetragonal}} \xrightarrow[\text{continuous}]{1403\,K} \text{cubic.}$$

Carlsson did not suggest space groups for these different structures, presumably because the superlattice peaks were not well defined in his work. Ahtee and co-workers (Ahtee *et al.*, 1976, 1978) used neutron powder diffraction to establish the room-temperature orthorhombic structure as that in *Pnma* ($a^+b^-b^-$) and recorded two diffraction patterns at elevated temperatures in an effort to establish the structures of the higher-temperature forms. They found the tetragonal phase to be that in *I*4/*mcm* ($a^0a^0c^-$), and for Carlsson's pseudo-tetragonal phase proposed the (orthorhombic) structure in *Cmcm* ($a^0b^+c^-$). There is little doubt that the high-temperature cubic phase would be the ideal perovskite, in space group $Pm\bar{3}m$. Ball *et al.* (1998) were no doubt influenced by Ahtee and co-workers in proposing the *Cmcm* structure for pseudo-tetragonal $Ca_{0.5}Sr_{0.5}TiO_3$ at room temperature, and in the course of temperature studies of the phase transitions in $SrZrO_3$, $SrHfO_3$ and $CaTiO_3$ (Kennedy *et al.*, 1999*a*,*b*,*c*), we too suggested this structure as a possible intermediate. It can be seen now that this was not a good choice for Carlsson's pseudo-tetragonal phase. Fig. 9 shows that a transition from the *Pnma* orthorhombic to *Cmcm* 'pseudo-tetragonal' could not be continuous, whereas the transition from *Cmcm* to tetragonal *I*4/*mcm* could and probably would be continuous, which would conflict with Carlsson's observations at both transitions.

Howard, Knight *et al.* (2000) re-examined the phase transitions in $SrZrO_3$, using very high resolution neutron powder diffraction, and working in fine temperature steps (as little as 5 K) from room temperature to 1503 K. They paid careful attention to both peak splitting and to the weak superlattice peaks. Like Carlsson, they found three transitions, at temperatures 1023, 1113 and 1343 K. The resolution was sufficient, and the temperature steps fine enough, to confirm the sudden reversal of tetragonal splitting at the second transition. It was noted that, at the first transition, the *R*-point reflections persisted, but the *M*-point reflections disappeared. This indicates the disappearance at this transition of the in-phase tilts. Starting from the *Pnma* ($a^+b^-b^-$) structure, and referring once more to Fig. 9, the only structure accessible by continuous transition and showing only out-of-phase tilts is that in *Imma* ($a^0b^-b^-$). This structure was confirmed by a Rietveld (1969) analysis. The results then can be summarized as

$$\underset{Pnma\,(a^+b^-b^-)}{\text{orthorhombic}} \xrightarrow[\text{continuous}]{1023\,K} \underset{\substack{Imma\\(a^0b^-b^-)\\b<a\sqrt{2}\approx c\sqrt{2}}}{\text{pseudo-tetragonal}} \xrightarrow[\text{discontinuous}]{1113\,K} \underset{\substack{I4/mcm\\(a^0a^0c^-)\\c>a\sqrt{2}}}{\text{tetragonal}} \xrightarrow[\text{continuous}]{1343\,K} \underset{\substack{Pm\bar{3}m\\(a^0a^0a^0)}}{\text{cubic}},$$

a sequence entirely consistent with both Carlsson's observations and the group-theoretical analysis. The lattice-parameter data obtained in this study are reproduced here in Fig. 15.

Exactly the same structural sequence has been found in a neutron study of $SrSnO_3$ (Glerup *et al.*, 2005), the transitions being at temperatures 905, 1062 and 1295 K, and it is considered likely that it will also be found in $SrHfO_3$. The sequence has also been reported in temperature studies of $SrRuO_3$ (Kennedy *et al.*, 2002) and in composition studies on the systems $Sr_{1-x}Ba_xSnO_3$ (Mountstevens *et al.*, 2003) and $Sr_{1-x}Ba_xHfO_3$ (Li *et al.*, 2004). We note that the sequence *Pnma* → *Imma* → $R\bar{3}c$ → $Pm\bar{3}m$ seen earlier in $BaCeO_3$ (Knight, 1994) can be considered closely analogous (Fig. 9) to the sequence occurring in $SrZrO_3$.

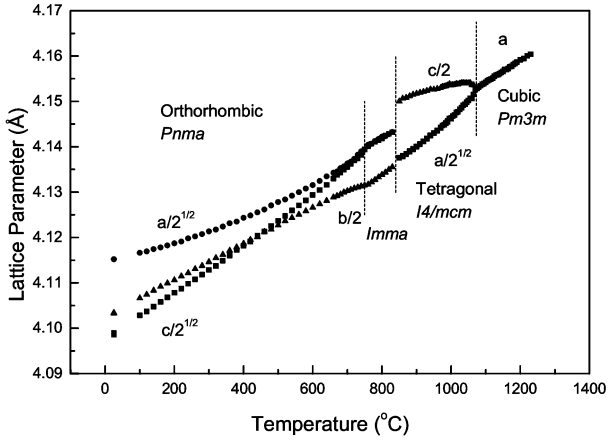

Figure 15
Temperature dependence of (suitably reduced) lattice parameters for $SrZrO_3$. The structure in *Imma* is described on the same cell as that in *Pnma*. This figure has been reproduced with permission from Howard, Knight, Kennedy & Kisi (2000). Copyright (2000). Institute of Physics Publishing.

4.4. Tungsten trioxide (WO_3)

Tungsten trioxide, WO_3, can be considered as an ABX_3 perovskite lacking the *A* cation. It adopts many different structures, characterized by an antiferroelectric pattern of W^{6+}-ion displacements and, except at the highest temperatures, WO_6 octahedral tilting. In reviewing the various studies of WO_3, it is convenient to make reference to the structure schematic shown here as Fig. 16.

Early X-ray studies established the structure at or just above room temperature as monoclinic, in $P2_1/n$ ($a^-b^+c^-$) (Tanisaki, 1960) and at the highest temperatures (~1273 K) tetragonal in *P*4/*nnm* ($a^0a^0c^0$) (Kehl *et al.*, 1952). In the high-temperature X-ray pattern, the *M*-point reflections associated with the W^{6+} displacement were easily seen. Anomalies in specific heat and lattice parameters gave strong indications of a structural phase transition at around 1173 K, but it is interesting to note that not until 1999, when the first neutron powder diffraction studies of the high-temperature phases were reported (Vogt *et al.*, 1999; Locherer *et al.*, 1999), was the nature of this transition understood. In effect, the neutron patterns recorded from tetragonal WO_3 below 1173 K showed *R*-point reflections, associated with out-of-phase octahedral tilting, which had not been seen using X-rays. The structure is that in *P*4/*ncc* ($a^0a^0c^-$). To cut a long story short (see Howard

et al., 2002, for the full account), after the 1999 neutron studies it would have been reasonable to conclude from the experimental studies that the sequence of structures above room temperature was

$$\underset{P2_1/n}{\text{monoclinic}} \xrightarrow[\text{continuous}]{603\text{ K}} \underset{Pbcn}{\text{orthorhombic}} \xrightarrow[\text{discontinuous}]{1013\text{ K}} \underset{P4/ncc}{\text{tetragonal}} \xrightarrow[\text{continuous}]{1183\text{ K}} \underset{P4/nnm}{\text{tetragonal.}}$$

Referring to Fig, 16, this sequence is not unreasonable, but puzzling to the extent that the transition at 1013 K, which in this sequence would be allowed to be continuous, is known to be strongly discontinuous in nature.

Howard *et al.* (2002) carried out a study, again using very high resolution neutron powder diffraction and fine temperature steps. A small selection of their diffraction patterns is shown in Fig. 17. They found a previously unrecognized monoclinic structure existing over a limited (~80 K) temperature range just below the $P4/ncc$ tetragonal, and transforming continuously to that tetragonal. From Fig. 16, there are only two candidate structures, those in $C2/c$ ($a^-b^0c^-$) and $P2_1/c$ ($a^-a^-c^-$), and it was relatively easy to establish that the observed monoclinic structure was the second of these. Other structures were confirmed as above, the sequence becoming

$$\underset{P2_1/n}{\text{monoclinic}} \xrightarrow[\text{continuous}]{623\text{ K}} \underset{Pbcn}{\text{orthorhombic}} \xrightarrow[\text{discontinuous}]{993\text{ K}} \underset{P2_1/c}{\text{monoclinic}} \xrightarrow[\text{continuous}]{1073\text{ K}} \underset{P4/ncc}{\text{tetragonal}} \xrightarrow[\text{continuous}]{1173\text{ K}} \underset{P4/nnm}{\text{tetragonal.}}$$

There being no group–subgroup relationship between the structures in $Pbcn$ and $P2_1/c$, the discontinuous nature of the transition from the orthorhombic phase was now just as expected. Although Howard *et al.* (2002) were first to identify a monoclinic phase between 993 and 1073 K, we note with interest that Kehl *et al.* (1952) commented on broadening of lines in the back-reflection region of X-ray patterns recorded in this temperature range, and that at similar temperatures there appear to be missing lattice-parameter data in the Locherer *et al.* (1999) report.

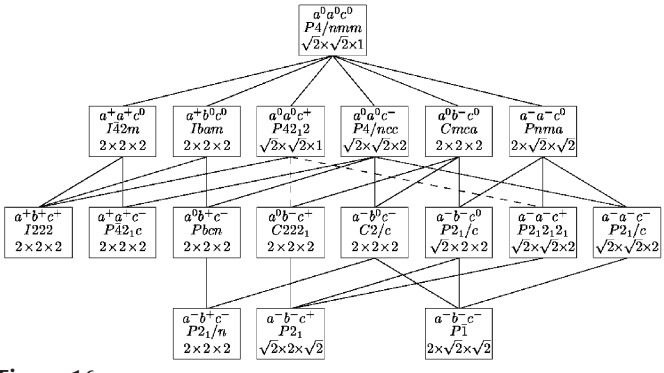

Figure 16
Schematic of structures relating to WO_3. The structures combine an antiferroelectric pattern of W^{6+} displacements, along with WO_6 tilting as indicated by the Glazer symbols. The group–subgroup relationships are shown in the usual way. This figure is essentially as displayed in the paper by Howard *et al.* (2002).

4.5. Lanthanum titanate ($La_{2/3}TiO_3$)

This is a perovskite with a partially occupied A site, the cations/vacancies being ordered in such a way that layers of A sites are alternately fully and one-third occupied by the La^{3+} ions. According to this description, the c repeat is doubled, yet the symmetry remains tetragonal, and the space-group symmetry should be $P4/mmm$. This was indeed the structure at temperatures above about 573 K, but the structure at room temperature was found to show a slight orthorhombic distortion (Abe & Uchino, 1974). Furthermore, synchrotron X-ray measurements on materials close to this composition indicate that the orthorhombic-to-tetragonal transition is continuous (Ali *et al.*, 2002; Yashima *et al.*, 2002). These X-ray measurements did not however lead to any reasonable model for the orthorhombic structure.

Howard & Zhang (2003) carried out high-resolution X-ray diffraction studies, under the prior assumption that the orthorhombic distortion would be due to octahedral tilting. The possible structures were enumerated using *ISOTROPY* (irreps X_3^-, M_3^+ and R_4^+), and (corrected) results have been presented by Howard & Zhang (2004*a*,*b*). There are only three orthorhombic structures, $a^+b^0c^0$ in $Pmmm$ on a $1\times2\times2$ cell, $a^-b^0c^0$ in $Cmmm$ on a $2\times2\times2$ cell, and $a^-a^-c^0$ in $Pmma$ on a $\sqrt{2}\times2\times\sqrt{2}$ cell related to the tetragonal $P4/mmm$ ($1\times2\times2$ cell) as a group–subgroup pair, and hence by a potentially continuous phase transition. The last can be excluded on the grounds that it does not give the triplet splitting (observed in the synchrotron studies) at the $h00$ reflections. The first would lead to weak superlattice reflections at the M points, and the second to reflections at the R points. Close examination of the X-ray patterns (recorded with very low background) revealed weak and previously unnoticed reflections at the R points, whence the structure in

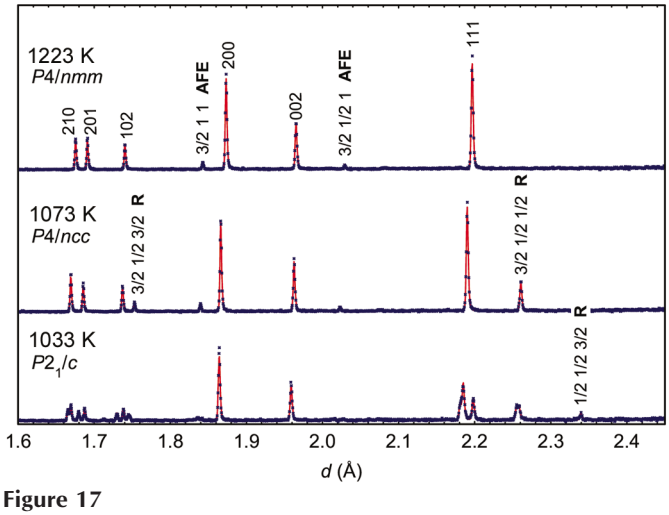

Figure 17
Extracts from the neutron diffraction patterns from WO_3 at selected temperatures. The crosses represent the measured patterns, while the continuous lines are fitted. The main peaks are identified by indices referred to the parent structure in $Pm\bar{3}m$, the X-point reflections are marked here as 'AFE', and the R-point reflections are marked as such. The pattern recorded at 1033 K is from a previously unrecognized monoclinic structure, existing over only a limited range of temperatures.

Cmmm was established then refined. The structure was determined, independently, without the group-theoretical analysis but using neutron powder diffraction, where the *R*-point reflections were readily seen (Inaguma *et al.*, 2002; Yashima *et al.*, 2003). Other *A*-site-deficient perovskites may adopt the same structure (Howard & Zhang, 2004*a*,*b*).

4.6. Structures of complex perovskites

We are unaware of any studies of complex perovskites at the level of detail seen in the preceding sections, and there has been only limited use of group theory in underpinning structural results.

One of the best studied is $BaBiO_3$, which is in effect the ordered double perovskite $Ba_2Bi^{3+}Bi^{5+}O_6$, by virtue of the charge ordering of the Bi ions.[12] The results from different authors (Cox & Sleight, 1976, 1979; Pei *et al.*, 1990) were collated by Howard *et al.* (2003) to suggest the sequence

$$\begin{array}{c} \text{monoclinic} \\ P2_1/c \\ (a^+b^-b^-) \end{array} \xrightarrow[\text{continuous}]{\sim 140\ \text{K}} \begin{array}{c} \text{monoclinic} \\ C2/m \\ (a^0b^-b^-) \end{array} \xrightarrow[\text{discontinuous}]{405\ \text{K}} \begin{array}{c} \text{rhombohedral} \\ R\bar{3} \\ (a^-a^-a^-) \end{array} \xrightarrow[\text{continuous}]{750\text{–}800\ \text{K}} \begin{array}{c} \text{cubic} \\ Fm\bar{3}m \\ (a^0a^0a^0) \end{array},$$

consistent with the scheme in Fig. 11. For the low-temperature phase, Pei *et al.* (1990) tentatively suggested $P2/m$ but, on the basis of Fig. 11, $P2_1/c$ was preferred. It is interesting to note that, as regards octahedral tilting, the suggested sequence exactly matches that seen in the simple perovskite $BaCeO_3$ (Knight, 1994).

A more systematic study of the double perovskite Sr_2MnTeO_6 was reported recently by Ortega-San Martin *et al.* (2004). These authors determined the room-temperature structure using neutron powder diffraction, then followed the temperature evolution using laboratory X-rays. The sequence they find is

$$\begin{array}{c} \text{monoclinic} \\ P2_1/c \\ (a^+b^-b^-) \end{array} \xrightarrow{\sim 523\ \text{K}} \begin{array}{c} \text{monoclinic} \\ C2/m \\ (a^0b^-b^-) \end{array} \xrightarrow{\sim 823\ \text{K}} \begin{array}{c} \text{tetragonal} \\ I4/m \\ (a^0a^0c^-) \end{array} \xrightarrow{\sim 948\ \text{K}} \begin{array}{c} \text{cubic} \\ Fm\bar{3}m \\ (a^0a^0a^0) \end{array},$$

again in accord with Fig. 11. It is apparent from this figure (or directly from consideration of the tilts) that the transition from the monoclinic in $C2/m$ to the tetragonal in $I4/m$ could not be continuous, but from the published data the nature of this transition is difficult to determine. In this compound, as regards octahedral tilting, the sequence matches that in $SrZrO_3$ (§4.3). We believe there is considerable scope for further detailed diffraction studies of phase transitions in complex perovskites.

We are aware of a few instances of the use of group theory, implemented in *ISOTROPY*, as an aid to structure determination. In a study of Sr_2FeMoO_6, Chmaissem *et al.* (2000) noted an apparently continuous phase transition from tetragonal to cubic in $Fm\bar{3}m$ at ~420 K, and after recourse to *ISOTROPY* concluded that the space group would be $I4/m$ (as in the example just above). Park & Woodward (2000) synthesized the perovskite $Ba_3TeBi_2O_9$ (1:2 *B*-site cation ordering, see §2.7), and determined its structure from a combination of synchrotron X-ray and neutron powder diffraction with analysis using *ISOTROPY*. The tilt system is $a^-a^-a^-$ and the space group $P\bar{3}c1$. By contrast, Woodward & Baba-Kishi (2002) had difficulty reconciling their proposed structure for the ferroelectric state of the relaxor oxide $Pb_2(ScTa)O_6$ with results from the group-theoretical analysis. As a final example, we note that the structure for ferroelectric $Pb(Ti_{0.48}Zr_{0.52})O_3$, first proposed as $a^0_+a^0_+c^-_+$ in space group Pc, was given as $a^-_+a^-_+c^-_+$ in space group Cc, following group-theoretical analysis (Hatch *et al.*, 2002).

5. Strains and order parameters

The focus in the previous section was on the determination of structures and structural sequences. Another facet of the phase-transition studies is the determination of order parameters. We will discuss this aspect only briefly here.

The order parameter is in effect a thermodynamic concept (Salje, 1990), but not without physical basis. In the case of ferroelectric *B*-cation displacements, the order parameter is measured by the cation displacements. For octahedral tilting, the tilt angle provides a measure of the order parameter. Phase transitions are classified according to the manner in which the order parameter (here denoted Q) varies as the transition is approached. Specifically, for temperature-induced phase transitions, the transition is second order, tricritical or first order, according as $Q^2 \propto (T_c - T)$, $Q^4 \propto (T_c - T)$ or Q changes discontinuously at the transition temperature T_c. In §2.2, we listed at equation (7) some terms in the free-energy expansion, but that expansion also contains elastic energy terms and terms coupling the strains to the order parameter(s). Equilibrium conditions of the kind $\partial G/\partial e = 0$ (e being a strain) give equations for the strain in terms of the order parameter, and hence it becomes possible to determine order parameters from measurements of the spontaneous strain. This strain is determined by the differences of lattice parameters measured in the lower-symmetry phase from the values they would take in the absence of the phase transition, the latter usually being obtained by extrapolation from measurements in the higher-symmetry phase. For octahedral tilting in simple perovskites, the full free-energy expansion (constructed with the aid of program *ISOTROPY*) and the strain–order-parameter relationships derived from it have been given by Carpenter *et al.* (2001). To summarize, the order parameter might be obtained from measurements of spontaneous strain, from distortions derived from internal atomic coordinates, or from both.

Lanthanum aluminate, $LaAlO_3$, is a perovskite, rhombohedral in $R\bar{3}c$ at room temperature, that undergoes a continuous transition to cubic in $Pm\bar{3}m$ at about 820 K. The tilt system in the rhombohedral phase is $a^-a^-a^-$, which means the tilt is around the [111] direction of the parent perovskite. There is only one variable atomic coordinate in the structure,

[12] *Footnote added in proof*. Kennedy *et al.* (in preparation) have just completed a detailed high-resolution neutron powder diffraction study of this compound. The low-temperature structure (below ~140 K) has been definitely established as the primitive monoclinic tilt system $a^+b^-b^-$ in space group $P2_1/c$. The sequence shown here has been confirmed.

the x parameter of the O atom, and the octahedral tilt angle ϕ is easily calculated from this. A neutron diffraction study (Howard, Kennedy & Chakoumakos, 2000) provided good estimates for the x parameter, and hence for the tilt angle, with the results shown in Fig. 18(a). Assuming ϕ measures the order parameter, and plotting ϕ^2 against temperature (Fig. 18b), we find reasonable linearity in the vicinity of the phase transition, so the transition is considered to be second order. The octahedral tilt angle in $LaAlO_3$ has also been estimated from electron paramagnetic resonance measurements (EPR) on a monodomain single crystal doped with Fe^{3+} (Müller *et al.*, 1968). The results from the neutron diffraction compare well with the earlier EPR results.

Although the spontaneous strains in perovskites tend to be small, the study of phase transitions in perovskites *via* these strains has been pursued by Carpenter and co-workers. Among the transitions examined in this way were the rhombohedral $R\bar{3}c$ to cubic $Pm\bar{3}m$ transition occurring at about 1170 K in $BaCeO_3$ (Carpenter *et al.*, 1998), the tetragonal $I4/mcm$ to cubic $Pm\bar{3}m$ transition in $CaTiO_3$ at 1580 K (Carpenter *et al.*, 2001), and in $PrAlO_3$ both the monoclinic $C2/m$ to orthorhombic *Imma* transition at 150 K and the rhombohedral $R\bar{3}c$ to cubic $Pm\bar{3}m$ transition at 1860 K (Carpenter *et al.*, 2005). From thermodynamic analyses, it was found that suitable symmetry-adapted strains should vary with Q for the $C2/m$ to *Imma* transition in $PrAlO_3$, and with Q^2 for the other transitions. The strains were found to depend approximately linearly on temperature for the transitions in $BaCeO_3$ and the 1860 K transition in $PrAlO_3$, whereas, for $CaTiO_3$ and the 150 K transition, the square of the strain was approximately linear in temperature. It was concluded that the transitions were second order in nature, except in the case of $CaTiO_3$ where the transition was considered to be tricritical. We believe the characterization of the 1860 K transition in $PrAlO_3$ as second order, based on analysis of spontaneous strains, is more reliable than the earlier suggestion (Howard, Kennedy & Chakoumakos, 2000) that this transition was tricritical.

The relationship between the spontaneous strains and physical order parameters, specifically octahedral tilting, was investigated as part of the study on $PrAlO_3$ (Carpenter *et al.*, 2005). These relationships were near to those expected. Spontaneous strain proved invaluable in a recent synchrotron X-ray study of the temperature-induced orthorhombic *Cmmm* to tetragonal $P4/mmm$ transition in $La_{1/3}NbO_3$ (Kennedy *et al.*, 2004). Octahedral tilt angles determined from atomic coordinates varied too erratically to permit any firm conclusion about the nature of the transition. The orthorhombic strain, however, is in this case expected to vary with Q^2, and the square of this strain was found to vary quite linearly with temperature. In this way, the transition was shown to be tricritical.

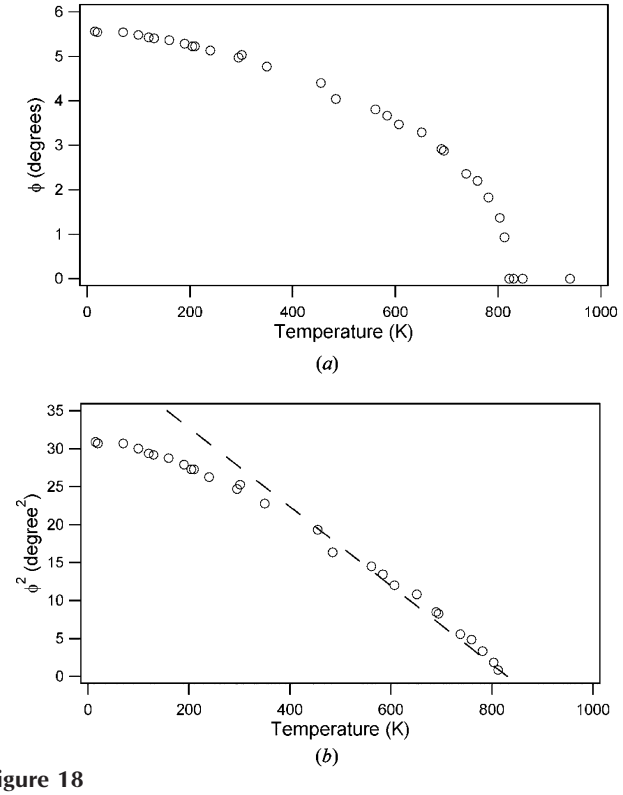

Figure 18
(a) The temperature dependence of the octahedral tilt angle in $LaAlO_3$. The tilt angle is calculated from the O-atom x parameter as determined by neutron diffraction. The square of this tilt angle, shown in (b), shows a nearly linear variation with temperature on approach to the phase transition, showing the transition to be second order. The departure of from linearity at low temperatures is attributed to saturation effects (Salje, 1990).

6. Summary and outlook

Structural variability in perovskites has long been known, and indeed the main types of distortions recognized long ago (Megaw, 1973). Cation or anion ordering is common. The various modifications can act separately or in combination. In this paper, we have shown how group representation theory can provide a basis for the systematic study of the various distortions, and the structures that result from them. We contend that this theory is now readily accessible *via* its implementation in the computer program *ISOTROPY*. In essence, three steps are involved – the first is the association of an irreducible representation with any given distortion, the second is the listing of isotropy subgroups for any irrep or combination of irreps, and the last is the identification of group–subgroup relationships and examination of group–subgroup pairs to see whether the corresponding phase transitions are allowed to be continuous. In the course of this work, we applied *ISOTROPY* to list the possible structures of elpasolites (ordered double perovskites) allowing both ferroelectric cation displacement and octahedral tilting. The *ISOTROPY* runs were completed and the possible structures listed within ten minutes, though the transcription of results into Table 2 took rather longer than this. There would seem to be few distortions, or combinations of distortions, that *ISOTROPY* could not readily address.

We reviewed a number of cases where the determination of the perovskite structures has been assisted by group-theor-

etical analysis. If the nature of the distortion is known, then the group-theoretical analysis will limit the possibilities. High-resolution X-ray or preferably neutron diffraction in fine steps of temperature may prove effective, since this provides a constraint on not just one structure but on a structural sequence. This methodology has been successful in resolving structural ambiguities in simple ABX_3 structures such as WO_3 and $SrZrO_3$, and we consider there is scope to study more complex perovskites (*e.g.* double perovskites) by this means. Finally, we described the monitoring of order parameters, using spontaneous strains calculated from lattice parameters, or physical distortions derived from atomic coordinates, or both.

Studies of perovskites are likely to continue, and in these further applications of *ISOTROPY* will be found. The application of group theory and *ISOTROPY*, however, has not been confined to the study of perovskites. Considerable attention has been given to structures containing layers of perovskite-type structure alternating with other structural motifs. Such structures are reviewed in ch. 7 of Mitchell's (2002) book. A number of authors have applied group-theoretical methods to examine the effect of octahedral tilting in such structures (Hatch & Stokes, 1987*a*,*b*; Aleksandrov & Bartolomé, 2001). A combination of ferroelectric cation displacements with octahedral tilting in layered perovskites has been analysed using *ISOTROPY* to assist in studies of temperature-induced phase transitions in $SrBi_2Ta_2O_9$ and $Ba_2Bi_2Nb_2O_9$ (Macquart, Kennedy, Hunter *et al.*, 2002; Macquart, Kennedy, Vogt & Howard, 2002). Similarly, the effects of different patterns of Fe^{2+}/Fe^{3+} charge ordering in $TbBaFe_2O_5$ were investigated using *ISOTROPY* as a step toward the determination of the crystal structure of this compound in its charge-ordered state (Karen *et al.*, 2001). The applications of *ISOTROPY* appear not to be limited by the complexity of the problems under consideration, but rather are to be found wherever the parent symmetry is high and the distortions more complex than are readily analysed by hand.

The work reviewed represents the efforts of many people, and we take this opportunity to acknowledge the contributions of our co-authors in papers cited below. CJH is particularly appreciative of long and fruitful collaborations with Brendan Kennedy, University of Sydney, Erich Kisi, University of Newcastle, Kevin Knight, ISIS Facility, and Michael Carpenter, Cambridge University. We thank Kevin Knight, Rene Macquart and Zhaoming Zhang for comments on the manuscript.

References

Abe, M. & Uchino, K. (1974). *Mater. Res. Bull.* **9**, 147–156.
Ahtee, A., Ahtee, M., Glazer, A. M. & Hewat, A. W. (1976). *Acta Cryst.* B**32**, 3243–32646.
Ahtee, M., Glazer, A. M. & Hewat, A. W. (1978). *Acta Cryst.* B**34**, 752–758.
Aleksandrov, K. S. (1976). *Ferroelectrics*, **14**, 801–805.
Aleksandrov, K. S. (1978). *Ferroelectrics*, **20**, 61–67.
Aleksandrov, K. S. & Bartolomé, J. (2001). *Phase Transitions*, **74**, 255–335.
Aleksandrov, K. S. & Misyul, S. V. (1981). *Sov. Phys. Crystallogr.* **26**, 612–618.
Ali., R., Yashima, M., Tanaka, M., Yoshioka, H., Mori, T. & Sasaki, S. (2002). *J. Solid State Chem.* **164**, 51–59.
Alonso, J. A., Mzyayek, E. & Rasines, I. (1990). *J. Solid State Chem.* **84**, 16–22.
Ball, C. J., Begg, B. D., Cookson, D. J., Thorogood, G. J. & Vance, E. R. (1998). *J. Solid State Chem.* **139**, 238–247.
Bärnighausen, H. (1975). *Acta Cryst.* A**31**, S3.
Beck, A., Bednorz, J. G., Gerber, Ch., Rossel, C. & Widmer, D. (2000). *Appl. Phys. Lett.* **77**, 139–141.
Bock, O. & Müller, U. (2002). *Acta Cryst.* B**58**, 594–606.
Burns, G. & Glazer, A. M. (1990). *Space Groups for Solid State Scientists*, 2nd ed. Boston: Academic Press.
Capponi, J. J., Chaillout, C., Hewat, A. W., Lejay, P., Marezio, M., Nguyen, N., Raveau, B., Soubeyroux, J. L., Tholence, J. L. & Tournien, R. (1987). *Europhys. Lett.* **3**, 1301–1307.
Carlsson, L. (1967). *Acta Cryst.* **23**, 901–905.
Carpenter, M. A., Becerro, A. I. & Seifert, F. (2001). *Am. Mineral.* **86**, 348–363.
Carpenter, M. A., Howard, C. J., Kennedy, B. J. & Knight, K. S. (2005). *Phys. Rev. B.* Submitted.
Carpenter, M. A. & Salje, E. K. H. (1998). *Eur. J. Mineral.* **10**, 693–812.
Carpenter, M. A., Salje, E. K. H. & Graeme-Barber, A. (1998). *Eur. J. Mineral.* **10**, 621–691.
Cava, R. J., van Dover, R. B., Batlogg, B. & Rietman, E. A. (1987). *Phys. Rev. Lett.* **58**, 408–410.
Chmaissem, O., Kruk, R., Dabrowski, B., Brown, D. E., Xiong, X., Kolesnik, S., Jorgensen, J. D. & Kimball, C. W. (2000). *Phys. Rev. B*, **62**, 14197–14206.
Cox, D. E. & Sleight, A. W. (1976). *Solid State Commun.* **19**, 969–973.
Cox, D. E. & Sleight, A. W. (1979). *Acta Cryst.* B**35**, 1–10.
Darlington, C. N. W., David, W. I. F & Knight, K. S. (1994). *Phase Transitions*, **48**, 217–236.
Darlington, C. N. W. & Knight, K. S. (1994). *Phase Transitions*, **52**, 261–275.
Frazer, B. C., Danner, H. R. & Pepinsky, R. (1955). *Phys. Rev.* **100**, 745–746.
Galasso, F. & Pyle, J. (1963). *Inorg. Chem.* **2**, 482–484.
Glazer, A. M. (1972). *Acta Cryst.* B**28**, 3384–3392.
Glazer, A. M. (1975). *Acta Cryst.* A**31**, 756–762.
Glerup, M., Knight, K. S. & Poulsen, F. W. (2005). *Mater. Res. Bull.* In the press.
Gong, G.-Q., Canedy, C., Xiao, G., Sun, J. Z., Gupta, A. & Gallagher, W. J. (1995). *Appl. Phys. Lett.* **67**, 1783–1785.
Hatch, D. M. (1984). *Group Theoretical Methods in Physics*, edited by G. Denardo, G. Ghirardi & T. Weber, pp. 390–393. New York: Springer.
Hatch, D. M., Kim, J. S., Stokes, H. T. & Felix, J. W. (1986). *Phys. Rev. B*, **33**, 6196–6209.
Hatch, D. M. & Stokes, H. T. (1985). *Phys. Rev. B*, **31**, 2908–2912.
Hatch, D. M. & Stokes, H. T. (1986). *Computer Modeling of Phase Diagrams*, edited by L. H. Bennett, pp. 145–162. Warrendale: American Metallurgical Society.
Hatch, D. M. & Stokes, H. T. (1987*a*). *Phys. Rev. B*, **35**, 8509–8516.
Hatch, D. M. & Stokes, H. T. (1987*b*). *Phys. Rev. B*, **36**, 7185.
Hatch, D. M., Stokes, H. T. & Putnam, R. M. (1987). *Phys. Rev. B*, **35**, 4935–4942.
Hatch, D. M., Stokes, H. T., Ranjan, R., Ragini, Mishra, S. K., Pandey, D. & Kennedy, B. J. (2002). *Phys. Rev. B*, **65**, 212101/1–3.
Hewat, A. W. (1974). *Ferroelectrics*, **6**, 215–218.
Howard, C. J., Kennedy, B. J. & Chakoumakos, B. C. (2000). *J. Phys. Condens. Matter*, **12**, 349–365.
Howard, C. J., Kennedy, B. J. & Woodward, P. M. (2003). *Acta Cryst.* B**59**, 463–471.

Howard, C. J., Knight, K. S., Kennedy, B. J. & Kisi, E. H. (2000). *J. Phys. Condens. Matter*, **12**, L677–L683.
Howard, C. J., Luca, V. & Knight, K. S. (2002). *J. Phys. Condens. Matter*, **14**, 377–387.
Howard, C. J., Lumpkin, G. R., Smith, R. I. & Zhang, Z. (2004). *J. Solid State Chem.* **177**, 2726–2732.
Howard, C. J. & Stokes, H. T. (1998). *Acta Cryst.* B**54**, 782–789.
Howard, C. J. & Stokes, H. T. (2002). *Acta Cryst.* B**58**, 565.
Howard, C. J. & Stokes, H. T. (2004). *Acta Cryst.* B**60**, 674–684.
Howard, C. J., Withers, R. L. & Kennedy, B. J. (2001). *J. Solid State Chem.* **160**, 8–12.
Howard, C. J. & Zhang, Z. (2003). *J. Phys. Condens. Matter*, **15**, 4543–4553.
Howard, C. J. & Zhang, Z. (2004*a*). *Acta Cryst.* B**60**, 249–251.
Howard, C. J. & Zhang, Z. (2004*b*). *Acta Cryst.* B**60**, 763.
Ibberson, R. M. David, W. I. F. & Knight, K. S. (1992). Report RAL 92–031. Rutherford Appleton Laboratory, Didcot, Oxon, England.
Inaguma, Y., Katsmata, T., Itoh, M. & Morii, Y. (2002). *J. Solid State Chem.* **166**, 67–72.
Jacobson, A. J., Collins, B. M. & Fender, B. E. F. (1974). *Acta Cryst.* B**30**, 1705–1711.
Jacobson, A. J., Collins, B. M. & Fender, B. E. F. (1976). *Acta Cryst.* B**32**, 1083–1087.
Karen, P., Woodward, P. M., Lindén, J., Vogt, T., Studer, A. & Fischer, P. (2001). *Phys. Rev. B*, **64**, 214405/1–14.
Kawashima, S., Nishida, M., Ueda, I. & Ouchi, H. (1983). *J. Am. Ceram. Soc.* **66**, 421–423.
Kay, H. F. & Bailey, P. C. (1957). *Acta Cryst.* **10**, 219–226.
Kay, H. F. & Vousden, P. (1949). *Philos. Mag.* **40**, 1019–1040.
Kehl, W. L., Hay, R. G. & Wahl, D. (1952). *J. Appl. Phys.* **23**, 212–215.
Kennedy, B. J., Howard, C. J. & Chakoumakos, B. C. (1999*a*). *Phys. Rev. B*, **60**, 2972–2975.
Kennedy, B. J., Howard, C. J. & Chakoumakos, B. C. (1999*b*). *Phys. Rev. B*, **59**, 4023–4027.
Kennedy, B. J., Howard, C. J. & Chakoumakos, B. C. (1999*c*). *J. Phys. Condens. Matter*, **11**, 1479–1488.
Kennedy, B. J., Howard, C. J., Kubota, Y. & Kato, K. (2004). *J. Solid State Chem.* **177**, 4552–4556.
Kennedy, B. J., Hunter, B. A. & Hester, J. R. (2002). *Phys. Rev. B*, **65**, 224103/1–4.
Kennedy, B. J., Prodjosantoso, A. K. & Howard, C. J. (1999). *J. Phys. Condens. Matter*, **11**, 6319–6327.
Knight, K. S. (1994). *Solid State Ionics*, **74**, 109–117.
Landau, L. D. & Lifshitz, E. M. (1980). *Statistical Physics*, 3rd ed., ch. XIV. New York: Pergamon Press.
Li, L., Kennedy, B. J., Kubota, Y., Kato, K. & Garrett, R. F. (2004). *J. Mater. Chem.* **14**, 263–273.
Locherer, K. B., Swainson, I. P. & Salje, E. H. K. (1999). *J. Phys. Condens. Matter*, **11**, 4143–4156.
Macquart, R., Kennedy, B. J., Hunter, B. A., Howard, C. J. & Shimakawa, Y. (2002). *Integrated Ferroelectrics*, **44**, 101–112.
Macquart, R., Kennedy, B. J., Vogt, T. & Howard, C. J. (2002). *Phys. Rev. B*, **66**, 212102/1–4.
Megaw, H. D. (1957). *Ferroelectricity in Crystals.* London: Methuen.
Megaw, H. D. (1973). *Crystal Structures – a Working Approach.* Philadelphia: W. B. Saunders.
Miller, S. C. & Love, W. F. (1967). *Tables of Irreducible Representations of Space Groups and Co-representations of Magnetic Space Groups.* Boulder: Pruett.
Mitchell, R. H. (2002). *Perovskites – Modern and Ancient.* Thunder Bay, ON: Almaz Press.
Mountstevens, E. H., Attfield, J. P. & Redfern, S. A. T. (2003). *J. Phys. Condens. Matter*, **15**, 8315–8326.
Moussa, S. M., Kennedy, B. J., Hunter, B. A., Howard, C. J. & Vogt, T. (2001). *J. Phys. Condens. Matter*, **13**, L203–L209.
Müller, K. A., Berlinger, W. & Waldner, F. (1968). *Phys. Rev. Lett.* **21**, 814–817.
Nagai, T., Sugiyama, M., Sando, M. & Niihara, K. (1997). *Jpn. J. Appl. Phys.* **36**, 1146–1153.
Newnham, R. E. (1998). *Acta Cryst.* A**54**, 729–737.
Ortega-San Martin, L., Chapman, J. P., Hernández-Bocanegra, E., Insausti, M., Arriortua, M. I. & Rojo, T. (2004). *J. Phys. Condens. Matter*, **16**, 3879–3888.
Park, J.-H. & Woodward, P. M. (2000). *Int. J. Inorg. Mater.* **2**, 153–166.
Pei, S., Jorgensen, J. D., Dabrowski, B., Hinks, D. G., Richards, D. R., Mitchell, A. W., Newsam, J. M., Sinha, S. K., Vaknin, D. & Jacobson, A. J. (1990). *Phys. Rev. B*, **41**, 4126–4141.
Rietveld, H. M. (1969). *J. Appl. Cryst.* **2**, 65–71.
Ringwood, A. E. (1962). *J. Geophys. Res.* **67**, 4005–4020.
Salje, E. H. K. (1990). *Phase Transitions in Ferroelastic and Co-elastic Crystals.* Cambridge University Press.
Shirane, G., Danner, H. & Pepinsky, R. (1957). *Phys. Rev.* **105**, 856–860.
Shirokov, V. B. & Torgashev, V. I. (2004). *Crystallogr. Rep.* **49**, 20–28.
Stokes, H. T. & Hatch, D. M. (1984). *Phys. Rev. B*, **30**, 4962–4967.
Stokes, H. T. & Hatch, D. M. (1985). *Phys. Rev. B*, **31**, 4700.
Stokes, H. T., Kisi, E. H., Hatch, D. M. & Howard, C. J. (2002). *Acta Cryst.* B**58**, 934–938.
Tanisaki (1960). *J. Phys. Soc. Jpn*, **15**, 573–581.
Ting, V., Liu, Y., Withers, R. L. & Norén, L. (2004). *J. Solid State Chem.* **177**, 2295–2304.
Thomas, N. W. (1989). *Acta Cryst.* B**45**, 337–344.
Thomas, N. W. (1996). *Acta Cryst.* B**52**, 16–31.
Vogt, T., Woodward, P. M. & Hunter, B. A. (1999). *J. Solid State Chem.* **144**, 209–215.
Woodward, P. M. (1997*a*). *Acta Cryst.* B**53**, 32–43.
Woodward, P. M. (1997*b*). *Acta Cryst.* B**53**, 44–66.
Woodward, P. M. (1997*c*). PhD thesis, Oregon State University, USA.
Woodward, P. M. & Baba-Kishi, K. Z. (2002). *J. Appl. Cryst.* **35**, 233–242.
Yashima, M., Ali, R., Tanaka, M. & Mori, T. (2002). *J. Am. Ceram. Soc.* **84**, 468–470.
Yashima, M., Mori, M., Kamiyama, T., Oikawa, K., Hoshikawa, A., Torii, S., Saitoh, K. & Tsuda, K. (2003). *Chem. Phys. Lett.* **375**, 240–246.